ARTICLES
https://doi.org/10.1038/s41556-018-0066-7
nature cell biology

GUARDIN is a p53-responsive long non-coding RNA that is essential for genomic stability

Wang Lai Hu[1,2,3,7], Lei Jin[4,7], An Xu[1,7], Yu Fang Wang[5], Rick F. Thorne[2,6], Xu Dong Zhang[2,4*] and Mian Wu[1,2*]

The list of long non-coding RNAs (lncRNAs) involved in the p53 pathway of the DNA damage response is rapidly expanding, but whether lncRNAs have a role in maintaining the de novo structure of DNA is unknown. Here, we demonstrate that the p53-responsive lncRNA GUARDIN is important for maintaining genomic integrity under steady-state conditions and after exposure to exogenous genotoxic stress. GUARDIN is necessary for preventing chromosome end-to-end fusion through maintaining the expression of telomeric repeat-binding factor 2 (TRF2) by sequestering microRNA-23a. Moreover, GUARDIN also sustains breast cancer 1 (BRCA1) stability by acting as an RNA scaffold to facilitate the heterodimerization of BRCA1 and BRCA1-associated RING domain protein 1 (BARD1). As such, GUARDIN silencing triggered apoptosis and senescence, enhanced cytotoxicity of additional genotoxic stress and inhibited cancer xenograft growth. Thus, GUARDIN may constitute a target for cancer treatment.

In response to sustained damage to DNA resulting from normal metabolic activities and environmental insults, such as radiation and thermal disruption, cells constantly activate the DNA damage response (DDR), a multifaceted array of biological processes that identifies and repairs DNA damage to facilitate cell survival and proliferation[1,2]. However, after excessive DNA damage and/or when repair is compromised, cells enter an irreversible state of dormancy (senescence), commit suicide (apoptosis) or, alternatively, cumulative genetic mutations can drive transformation[3–5].

To maintain genomic integrity, the ends of chromosomes must also be protected from recognition as double-strand DNA breaks[6]. This occurs through shelterin, a six protein complex that caps telomeres and prevents chromosome end-to-end fusions through inhibiting homologous recombination (HR) and non-homologous end joining (NHEJ)[7]. Shelterin component proteins comprise telomeric repeat-binding factor 1 (TRF1) and TRF2 that bind to duplex telomeric DNA and recruit protection of telomere 1 (POT1), repressor activator protein 1 (RAP1), TRF1- and TRF2-interacting nuclear protein 2 (TIN2) and tripeptidyl-peptidase 1 (TPP1) to telomeres through protein–protein interactions[8]. Defects in the shelterin complex trigger activation of the DDR, which leads to cell cycle arrest and apoptosis[9–11].

An important DDR component is the tumour suppressor p53, which facilitates DNA repair through cell cycle arrest and eliminates cells with severe DNA damage via the induction of apoptosis[12]. The transcriptional targets of p53 comprise a broad repertoire of protein-coding genes, and recent studies have revealed that many non-coding RNAs, including long non-coding RNAs (lncRNAs), are involved in regulating p53-dependent responses to DNA damage[13–18]. However, whether lncRNAs are involved in guarding the de novo structure of DNA in cells without exposure to exogenous genotoxic insults remains unexplored.

Here, we demonstrate that the p53-responsive lncRNA GUARDIN is not only important for maintaining genomic stability in cells exposed to genotoxic stress but also under steady-state conditions. GUARDIN acts pleiotropically to maintain TRF2 expression levels by sequestering microRNA-23a (miR-23a) and through sustaining breast cancer 1 (BRCA1) expression by acting as a scaffold that facilitates the heterodimerization of BRCA1 with BRCA1-associated RING domain protein 1 (BARD1). Moreover, we show that GUARDIN is essential for cell survival and proliferation, with practical implications of interference with GUARDIN in cancer treatment.

Results

Identification of GUARDIN as a p53-responsive lncRNA. We took advantage of *TP53*-null H1299 human lung adenocarcinoma cells carrying an inducible wild-type p53 expression system to interrogate lncRNAs that are responsive to p53 using array profiling (ref. [13]). Five identified lncRNAs that are triggered by p53 were validated by quantitative PCR along with the previously reported p53-responsive lncRNAs lincRNA-p21 and DINO[14,15], (Supplementary Table 1 and Supplementary Fig. 1a). Strikingly, knockdown of lncRNA#6 in wild-type p53-expressing HCT116 cells, but not other lncRNAs, led to reduced cell viability and activation of caspase 3 (Supplementary Fig. 1b–d). Bioinformatics analysis revealed that lncRNA#6 corresponds to lncRNA RP3-510D11.2 with three annotated isoforms (Vega Genome Browser). Nevertheless, the longest isoform RP3-510D11.2-1 appeared markedly more abundant than the others (RP3-510D11.2-2 and RP3-510D11.2-3) even when p53 was induced (Supplementary Fig. 1e). Thus, we focused on RP3-510D11.2-1 and, for simplicity, refer to this isoform as GUARDIN given its functional relationship with p53, the guardian of the genome.

[1]Chinese Academy of Sciences (CAS) Key Laboratory of Innate Immunity and Chronic Disease, CAS Centre for Excellence in Cell and Molecular Biology, Innovation Centre for Cell Signalling Network, School of Life Sciences, University of Science and Technology of China, Hefei, China. [2]Translational Research Institute, Henan Provincial People's Hospital, Zhengzhou, China. [3]Department of Immunology, Anhui Medical University, Hefei, China. [4]School of Medicine and Public Health, University of Newcastle, Callaghan, New South Wales, Australia. [5]Department of Pathophysiology, School of Preclinical and Forensic Medicine, Sichuan University, Chengdu, China. [6]School of Environmental and Life Sciences, University of Newcastle, Newcastle, New South Wales, Australia. [7]These authors contributed equally: Wang Lai Hu, Lei Jin, An Xu. *e-mail: Xu.Zhang@newcastle.edu.au; wumian@ustc.edu.cn

We extended our analysis to multiple lines, confirming that overexpression of wild-type p53 in U2OS osteosarcoma, A549 lung adenocarcinoma and HCT116 cells increased GUARDIN levels, whereas knockdown of p53 decreased GUARDIN expression (Fig. 1a,b). Moreover, activation of the DDR with doxorubicin or overexpression of the oncogenic $HRAS^{V12}$ mutant led to GUARDIN upregulation in malignant cells and in untransformed adult foreskin fibroblasts (HAFFs)[16] (Fig. 1c,d). Increased GUARDIN expression was prevented when p53 was silenced (Fig. 1e,f), indicating that GUARDIN induction during the DDR was p53 dependent. In support, damage to DNA caused by ionizing radiation or the p53 activator nutlin 3a upregulated GUARDIN in MCF-7 breast cancer cells[17]. GUARDIN was not increased in H1299 cells transduced with p53 mutants (p53-R175H and p53-R273H)[18–20] (Supplementary Fig. 1e), further highlighting the importance of wild-type p53 activity in transcriptional regulation of GUARDIN. In accordance, pifithrin-α (PFTα), a small-molecule inhibitor of p53 transcriptional activity[21], reduced GUARDIN levels along with $p21^{WAF1/Cip1}$ (Fig. 1g).

GUARDIN is located between the genes encoding miR-34a and hexose-6-phosphate dehydrogenase/glucose 1-dehydrogenase (H6PD) (Supplementary Fig. 2a). Intriguingly, this region is part of the *FRA1A* (aphidicolin type, common, Fra(1)(P36)) fragile site that is frequently lost in human cancers[22,23] (Supplementary Fig. 2a). Moreover, *GUARDIN* and the miR-34a host gene *MIR34AHG* overlap and share the same promoter (Supplementary Fig. 2a). Indeed, GUARDIN expression positively correlates with the expression of miR-34a and MIR34AHG, and transcripts were concurrently reduced in a proportion of colon cancers with gene copy number loss (Supplementary Fig. 2b,c and Supplementary Table 2). Neither silencing nor overexpression of GUARDIN altered the expression of miR-34a, its target Snail as well as MIR34AHG[24] (Supplementary Fig. 2d), indicating that GUARDIN has no role in regulating miR-34a expression. Conversely, neither miR-34a nor MIR34AHG affected GUARDIN expression (Supplementary Fig. 2e).

The promoter of the *GUARDIN* and *MIR34AHG* genes contains a consensus p53-binding region (p53-BR) (Supplementary Fig. 2f), which co-precipitated with endogenous p53 (Fig. 1h). Indeed, this region was required for p53-mediated GUARDIN upregulation, as the transcriptional activity of luciferase reporters containing intact p53-BR (−305/−329) was markedly stronger than those with the p53-BR deleted (Fig. 1i). Moreover, co-transfection of wild-type p53 selectively enhanced the transcriptional activity of reporters with intact p53-BR (Fig. 1i), whereas knockdown of p53 diminished reporter activity (Fig. 1j). Collectively, these data support the transactivation of GUARDIN by p53, acting through the identified p53-BR.

In accordance with the relationship between GUARDIN expression and p53 identified in vitro (Fig. 1), in situ analysis of two independent cohorts demonstrated that colon cancers with wild-type p53 expressed higher levels of GUARDIN than those carrying mutant p53 (Fig. 2a–c, Supplementary Fig. 2g and Supplementary Tables 2,3). Moreover, analysis of The Cancer Genome Atlas (TCGA) showed that GUARDIN (RP3-510D11.2) expression was broadly reduced in mutant *TP53* tumours[25]. There were no significant differences in GUARDIN expression between different colon cancer stages (Supplementary Table 3), although a subset displayed reduced GUARDIN levels compared with paired adjacent normal colonic epithelia, which was closely associated with copy number loss of *GUARDIN* and mutations in *TP53* (Fig. 2d). Of note, GUARDIN expression in colon cancers without copy number loss, similar to the expression of *CDKN1A* (which encodes p21) mRNA, was lower in mutant *TP53* cases than in paired pre-neoplastic epithelia (hyperplastic polyps and adenomas). Conversely, there were no significant differences in *GUARDIN* and *CDKN1A* mRNA expression between pre-neoplastic and paired normal colon epithelia (Supplementary Fig. 2h), together suggesting that GUARDIN, similar to p21, may represent an indicator of p53 activation[26,27]. In support, GUARDIN expression along with p21 was positively correlated with p53 expression in wild-type p53 colon cancers (Fig. 2e).

GUARDIN is essential for cell survival and proliferation. We next returned to evaluate the role of GUARDIN in the regulation of cell viability (Supplementary Fig. 1c,d). GUARDIN knockdown in HCT116, U2OS and A549 cells induced striking inhibition of proliferation that primarily resulted from loss of viability through induction of apoptosis[28] (Fig. 3a and Supplementary Fig. 3a–c). In addition, depletion of GUARDIN triggered cellular senescence[29,30] (Fig. 2b). These results support the notion that GUARDIN has an important role in survival and proliferation by antagonizing cellular stress that is constitutively present in cells[31]. The effects of GUARDIN on cell viability were mirrored in the long-term survival of HCT116 cells in clonogenic assays and in their growth in nu/nu mice (Fig. 3c–e).

To clarify the functional relationship between GUARDIN and p53, we depleted GUARDIN in H1299 cells bearing inducible wild-type p53 (Fig. 3f). Although GUARDIN knockdown in the absence of p53 did not significantly affect cell viability, cell death was enhanced following induction of p53 (Fig. 3f). Conversely, overexpression of GUARDIN diminished the reduction in cell viability associated with p53 induction (Fig. 3g). Thus, although p53 controls the function of GUARDIN through regulating its expression, GUARDIN modulates the cytotoxic effect of p53.

GUARDIN stabilizes TRF2 through sequestering miR-23a. GUARDIN primarily localizes to the cytoplasm (Fig. 4a), which suggests a possible function as a competitive endogenous RNA, acting as a molecular sponge for miRNAs[32,33]. A search of the miRDB database (http://www.mirdb.org/miRDB) showed that GUARDIN contained eight regions complementary to the 'seed' region of miR-23a, one region matching seven bases, another two matching six bases and a further five matching five bases (Supplementary Fig. 3d).

To establish whether miR-23a binds to GUARDIN, luciferase reporters containing GUARDIN (GUARDIN-WT) or a construct with the three most complementary miR-23a-BRs mutated were introduced into HCT116 cells (Supplementary Fig. 3e). Reporter activity was markedly suppressed in the presence of GUARDIN-WT, but not when the predicted miR-23a-BRs were mutated (Fig. 4b). Notably, introduction of miR-23a mimics or anti-miR-23a selectively reduced or alternatively increased reporter activity of GUARDIN-WT, respectively (Fig. 4b,c). Seeking further evidence for this interaction, we showed that in vitro-synthesized miR-23a mimics precipitated endogenous GUARDIN (Fig. 4d), and conversely, in vitro-synthesized GUARDIN associated with endogenous miR-23a but not a control (miR-202) (Fig. 4e). Moreover, miR-23a was co-precipitated by antisense probes directed to GUARDIN (Fig. 4f), collectively substantiating the selective interaction between GUARDIN and miR-23a. GUARDIN associated with in vitro-synthesized miR-23a from purified cytoplasmic, but not in nuclear, fractions (Fig. 4g), indicating that the endogenous GUARDIN–miR-23a interaction occurs largely in the cytoplasm. Absolute quantitation of GUARDIN and miR-23a by digital droplet PCR showed that there were ~70–150 GUARDIN molecules per cell versus ~180–400 molecules of miR-23a[34] (Fig. 4h).

One of the targets of miR-23a is TRF2 (ref. [35]), a critical component of the shelterin complex[36]. Strikingly, GUARDIN knockdown downregulated, whereas its overexpression upregulated, TRF2 along with another miR-23a target, interferon regulatory factor 1 (IRF1)[37] (Fig. 4i,j). Moreover, co-introduction of anti-miR-23a abolished the inhibitory effect of GUARDIN knockdown on TRF2 and IRF1 expression (Fig. 4k). These results suggest that GUARDIN functions to regulate TRF2 and IRF1 through sequestering miR-23a. The downregulation of TRF2 and IRF1 that accompanies

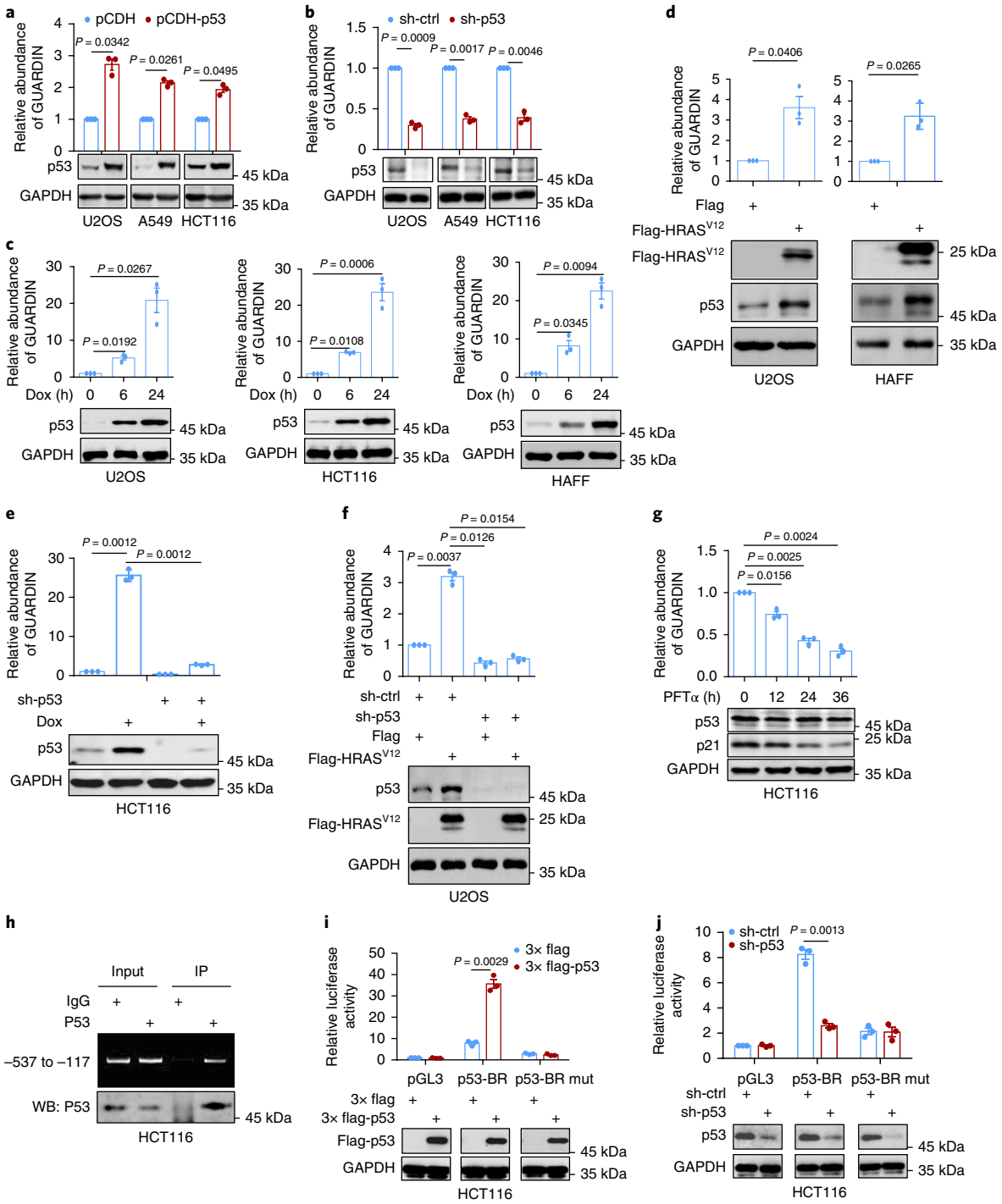

Fig. 1 | Identification of GUARDIN as a p53-inducible lncRNA. a, GUARDIN expression in U2OS, A549 and HCT116 cells transduced with empty vector (pCDH) or pCDH-p53. Data are shown as mean ± s.e.m.; $n = 3$ independent experiments, two-tailed Student's *t*-test. **b**, GUARDIN expression in U2OS, A549 and HCT116 cells transduced with the control (sh-ctrl) or p53 (sh-p53) shRNA. Data are shown as mean ± s.e.m.; $n = 3$ independent experiments, two-tailed Student's *t*-test. **c**, Treatment with doxorubicin (Dox) upregulated GUARDIN along with p53 in U2OS, HCT116 and HAFF cells. Data are shown as mean ± s.e.m.; $n = 3$ independent experiments, two-tailed Student's *t*-test. **d**, Enforced expression of $HRAS^{V12}$ upregulated GUARDIN in U2OS and HAFF cells. Data are shown as mean ± s.e.m.; $n = 3$ independent experiments, two-tailed Student's *t*-test. **e**, shRNA knockdown of p53 diminished GUARDIN upregulation caused by treatment with doxorubicin in HCT116 cells. Data are shown as mean ± s.e.m.; $n = 3$ independent experiments, two-tailed Student's *t*-test. **f**, shRNA knockdown of p53 diminished GUARDIN upregulation caused by enforced expression of $HRAS^{V12}$ in U2OS cells. Data are shown as mean ± s.e.m.; $n = 3$ independent experiments, two-tailed Student's *t*-test. **g**, Treatment with PFTα reduced GUARDIN expression and downregulated p21 without affecting the expression of p53 in HCT116 cells. Data are shown as mean ± s.e.m.; $n = 3$ independent experiments, two-tailed Student's *t*-test. **h**, p53 bound to the –537/–117 fragment of the *GUARDIN* gene promoter. Data shown represent three independent experiments. IP, immunoprecipitation; WB, western blot. **i**,**j**, Overexpression of p53 in the p3XFLAG-myc-CMV vector increased (**i**), whereas knockdown of p53 diminished (**j**), the transcriptional activity of reporter constructs with intact p53-BR but not reporters lacking the p53-BR. Data are shown as mean ± s.e.m.; $n = 3$ independent experiments, two-tailed Student's *t*-test. Blotting for GAPDH was used throughout as a loading control. Statistics source data for **a**–**g**,**i** and **j** are provided in Supplementary Table 7. Uncropped images of blots for **a**–**j** are shown in Supplementary Fig. 7.

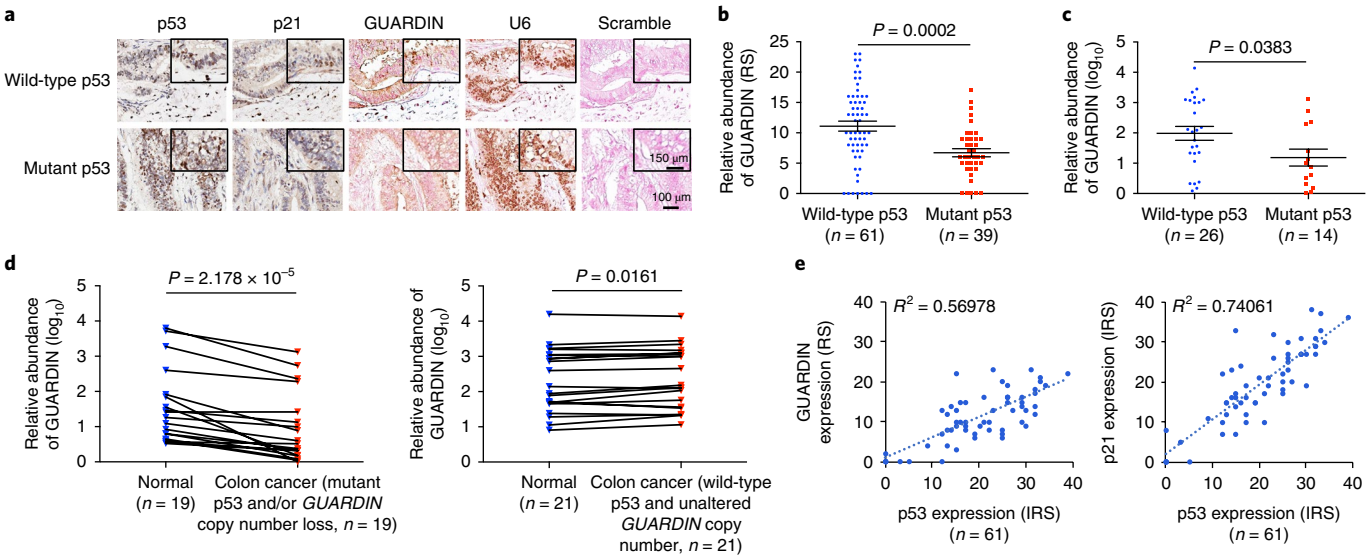

Fig. 2 | GUARDIN is expressed at higher levels in colon cancers with wild-type p53 than in those carrying mutant p53. a,**b**, GUARDIN (**a**,**b**) along with p21 (**a**) were expressed at higher levels in FFPE colon cancers with wild-type p53 ($n = 61$ biologically independent samples) than in those carrying mutant p53 ($n = 39$ biologically independent samples). Data are shown as mean ± s.e.m.; two-tailed Student's *t*-test. Data shown represent two independent experiments. RS, reactive score. **c**, GUARDIN was expressed at higher levels in laser capture microdissected (LCM) colon cancer cells from freshly removed tumours with wild-type p53 ($n = 26$ biologically independent samples) than in those carrying mutant p53 ($n = 14$ biologically independent samples). Data are shown as mean ± s.e.m.; two-tailed Student's *t*-test. **d**, GUARDIN expression was reduced in LCM colon cancer cells from freshly removed tumours with *GUARDIN* gene copy number loss and/or mutations in p53 ($n = 19$ biologically independent samples) compared with paired LCM adjacent normal epithelial cells; two-tailed Student's *t*-test. **e**, GUARDIN expression (left), similar to the expression of p21 (right), was positively correlated with p53 expression in FFPE colon cancers carrying wild-type p53 ($n = 61$ biologically independent samples); linear regression analysis. IRS, immunoreactive score. Statistics source data for **b**–**e** are provided in Supplementary Table 7.

GUARDIN knockdown was not affected by the proteasome inhibitor MG-132 (Fig. 4k), thereby excluding proteasomal involvement.

GUARDIN interacts with BRCA1 and BARD1 and is essential for the stabilization of BRCA1. Seeking to define the protein interactome of GUARDIN using mass spectrometry, we identified that BRCA1 precipitated with biotin-labelled GUARDIN (Fig. 5a). Western blotting confirmed that BRCA1 along with BARD1, a binding partner of BRCA1 that is necessary for BRCA1 stabilization[38,39], occurred within GUARDIN precipitates (Fig. 5b). Consistently, these interactions were readily detected using electrophoretic mobility shift assays (Supplementary Fig. 4a). Moreover, GUARDIN along with BARD1 co-immunoprecipitated with BRCA1 (Fig. 5c), consistent with the notion of a ternary complex. To substantiate this, we introduced Myc-tagged BRCA1 into HCT116 cells and used two-step RNA immunoprecipitation (RIP) assays. As expected, antibodies against the Myc epitope tag precipitated BRCA1 along with BARD1 and GUARDIN from total protein extracts, whereas in second-phase immunoprecipitation, anti-BARD1 antibodies co-precipitated BRCA1 and GUARDIN (Fig. 5d).

Strikingly, GUARDIN depletion resulted in marked reduction in BRCA1 expression, which recapitulated the effects of BARD1 knockdown (Fig. 5e). This was attributable to proteasomal degradation as BRCA1 levels were stabilized by MG132 (Fig. 5f). Moreover, GUARDIN knockdown increased the polyubiquitination of BRCA1 (Fig. 5g). Thus, GUARDIN is important for BRCA1 stabilization. Notably, GUARDIN knockdown diminished the relative amount of BRCA1 that associated with BARD1 (Fig. 5h,i), indicating that GUARDIN is required for their interaction. Indeed, GUARDIN promoted binding between purified BRCA1 and BARD1 in a cell-free system (Fig. 5j).

We carried out deletion-mapping experiments with GUARDIN mutants transcribed in vitro (Supplementary Fig. 4b). Although deletion of exon 3 diminished binding of GUARDIN to BARD1, deletion of either exon 1 or exon 2 prevented the association between GUARDIN with BRCA1 (Supplementary Fig. 4c,d). Thus, GUARDIN functions as an RNA scaffold for the association between BRCA1 and BARD1, with its fragments corresponding to exon 3, and exon 1 and exon 2 responsible for its association with BARD1 and BRCA1, respectively (Supplementary Fig. 4c,d). Deletion-mapping experiments with mutants of BRCA1 and BARD1 indicated that removing the BRCA1 amino terminus but not other regions abolished its association with GUARDIN (Supplementary Fig. 5a–c). Similarly, deletion of the N terminus of BARD1 also diminished its interaction with GUARDIN (Supplementary Fig. 5d). Thus, the GUARDIN-binding segments of BRCA1 and BARD1 occur within their N termini and do not overlap with the RING domains of BRCA1 and BARD1, which mediate the BRCA1–BARD1 interaction[40,41] (Supplementary Fig. 5e,f).

GUARDIN protects genomic integrity through TRF2 and BRCA1. We evaluated the global effects of GUARDIN on DNA damage using comet assays in which knockdown of GUARDIN caused the appearance of tails, phenocopying DNA damage caused by doxorubicin (Fig. 6a). Furthermore, knockdown of GUARDIN resulted in telomere fusion (Fig. 6b), the formation of phosphorylated histone H2AX (γH2A.X) foci (Fig. 6c) and the accumulation of p53-binding protein 1 (53BP1) co-localized with TRF1 (Fig. 6d), representative of the recruitment of DDR components to telomere ends[35]. These results suggest that GUARDIN is required to maintain genomic integrity with tonic activation of GUARDIN protecting telomeres and modulating DNA repair in response to damage that occurs constantly in cells[31].

We also assessed whether GUARDIN is involved in HR and NHEJ repair signalling[41]. The introduction of I-SceI expression constructs into U2OS-HR and U2OS-NHEJ cells provides a measure of the HR and NHEJ repair pathways, respectively, as measured by green fluorescent protein (GFP)-positive cells. Notably cells that

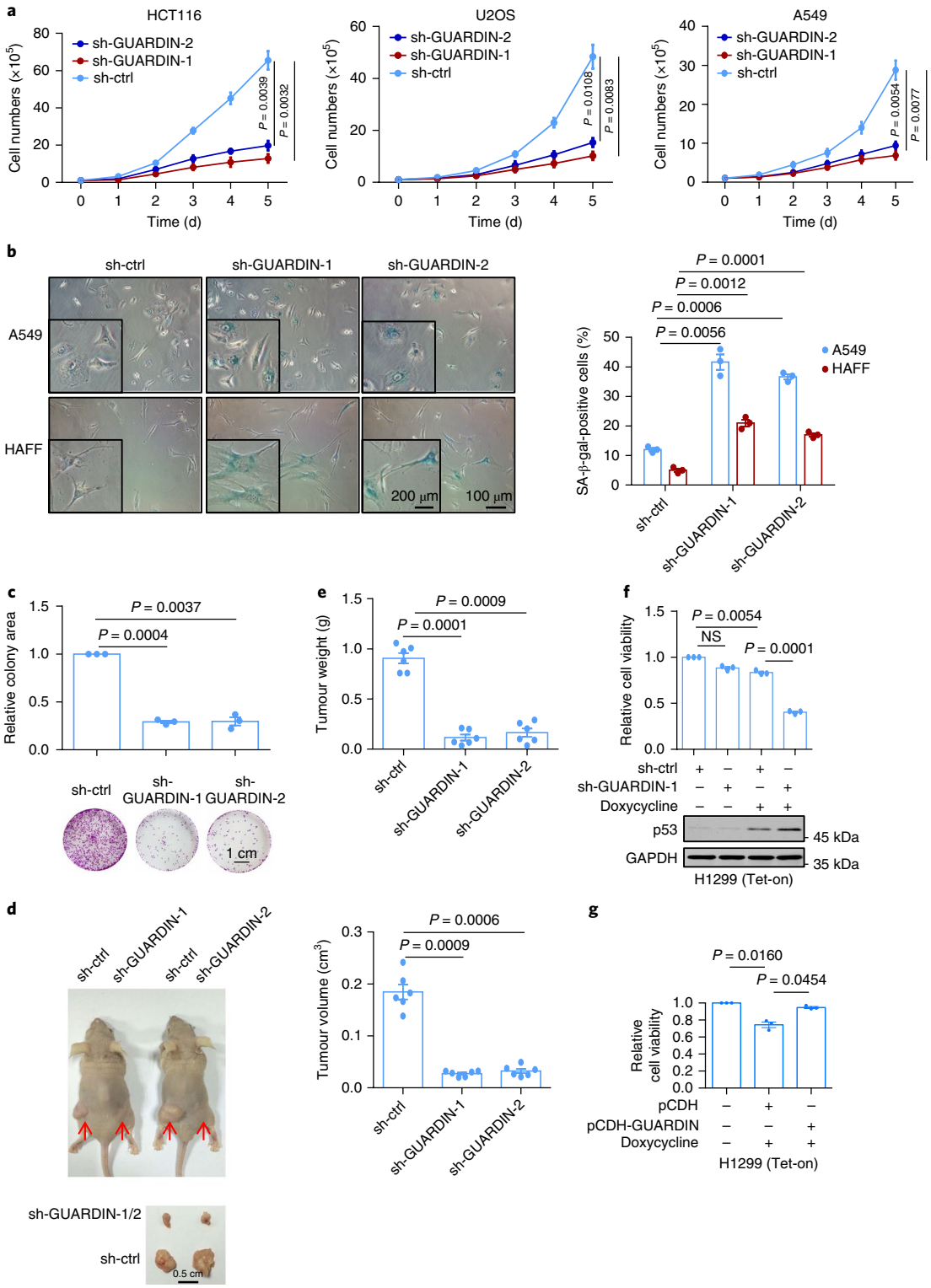

Fig. 3 | GUARDIN is important for cell survival and proliferation. a, Silencing of GUARDIN inhibited cell number expansion in HCT116, U2OS and A549 cells. d, days. Data are shown as mean ± s.e.m.; $n = 3$ independent experiments, two-tailed Student's t-test. **b**, Silencing of GUARDIN for 48 h induced senescence in A549 and HAFF cells. Data are shown as mean ± s.e.m.; $n = 3$ independent experiments, two-tailed Student's t-test. SA-β-gal-positive, senescence-associated β-galactosidase-positive. **c**, Silencing of GUARDIN inhibited the clonogenic potential of HCT116 cells. Data are shown as mean ± s.e.m.; $n = 3$ independent experiments, two-tailed Student's t-test. **d**,**e**, Silencing of GUARDIN inhibited HCT116 xenograft growth in nu/nu mice. Arrows denote tumours in situ. Data are shown as mean ± s.e.m.; $n = 6$ mice per group, two-tailed Student's t-test. Data shown represent two independent experiments. **f**, Silencing of GUARDIN in H1299 cells carrying an inducible wild-type p53 expression system did not affect cell viability in the absence of p53, but enhanced cell death resulting from p53 induction. Data are shown as mean ± s.e.m.; $n = 3$ independent experiments, two-tailed Student's t-test. **g**, Overexpression of GUARDIN diminished the reduction in cell viability caused by p53 induction in H1299 cells carrying an inducible wild-type p53 expression system. Data are shown as mean ± s.e.m.; $n = 3$ independent experiments, two-tailed Student's t-test. Statistics source data for **a**–**c** and **e**–**g** are provided in Supplementary Table 7. Uncropped images of blots for **f** are shown in Supplementary Fig. 7.

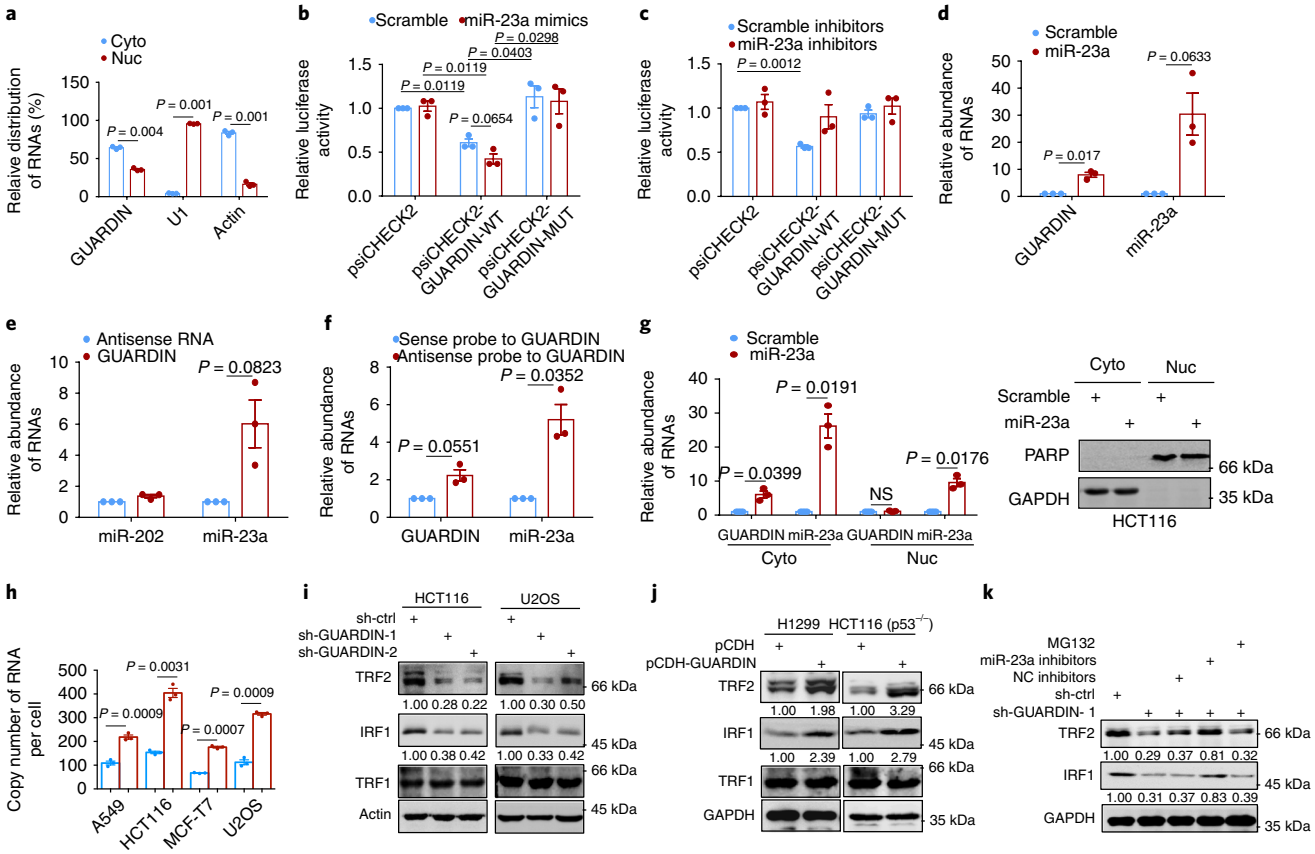

Fig. 4 | GUARDIN sequesters miR-23a to stabilize TRF2. a, Relative GUARDIN expression levels in the cytoplasmic (cyto) and nuclear (nuc) fractions of HCT116 cells. Data are shown as mean ± s.e.m.; $n = 3$ independent experiments. **b**,**c**, miR-23a mimics inhibited (**b**), whereas miR-23a inhibitors promoted (**c**), the activity of report constructs of GUARDIN with intact miR-23a-BRs but not reporters with the three predicted miR-23a-BRs mutated. Data are shown as mean ± s.e.m.; $n = 3$ independent experiments, two-tailed Student's *t*-test. **d**, GUARDIN was pulled down with in vitro-synthesized biotin-labelled miR-23a. Data are shown as mean ± s.e.m.; $n = 3$ independent experiments, two-tailed Student's *t*-test. **e**, miR-23a was pulled down with in vitro-transcribed biotin-labelled GUARDIN but not GUARDIN antisense RNA. Pulldown of miR-202 was included as a control. Data are shown as mean ± s.e.m.; $n = 3$ independent experiments, two-tailed Student's *t*-test. **f**, miR-23a was pulled down by antisense but not sense probes directed to GUARDIN. Data are shown as mean ± s.e.m.; $n = 3$ independent experiments, two-tailed Student's *t*-test. **g**, In vitro-synthesized biotin-labelled miR-23a pulled down GUARDIN in the cytoplasmic but not the nuclear fraction of HCT116 cells. The purity of cytoplasmic and nuclear fractions is also shown. Data are shown as mean ± s.e.m.; $n = 3$ independent experiments, two-tailed Student's *t*-test. **h**, Quantitation of copy numbers of GUARDIN (blue) and miR-23a (red) in individual cells. Data are shown as mean ± s.e.m.; $n = 3$ independent experiments, two-tailed Student's *t*-test. **i**, Silencing of GUARDIN caused downregulaton of TRF2 and IRF1 but not TRF1 in HCT116 and U2OS cells. Data are shown represent three independent experiments. **j**, Overexpression of GUARDIN caused upregulation of TRF2 and IRF1 but not TRF1 in p53-null H1299 and p53-knockout HCT116 cell sublines. Data shown represent three independent experiments. **k**, Downregulation of TRF2 caused by silencing of GUARDIN was reversed by miR-23a inhibitors but not by the proteasome inhibitor MG132. NC, negative control (scrambled sequence). Data shown represent three independent experiments. Statistics source data for **a**–**h** are provided in Supplementary Table 7. Uncropped images of blots for **g** and **i**–**k** are shown in Supplementary Fig. 7.

were depleted of GUARDIN displayed a marked reduction in the number of GFP-positive cells in both U2OS-HR and U2OS-NHEJ assays (Fig. 6e). This was associated with cell cycle arrest in the G0/G1 phase (Supplementary Fig. 6a), but was not due to apoptosis or senescence, as reduction in HR and NHEJ was detectable at 24 h (Fig. 6e), which is well before apoptosis and senescence could be detected at 48 h after GUARDIN knockdown (Fig. 3a,b). In addition, inhibition of apoptosis by z-VAD-fmk did not affect the reduction in HR and NHEJ resulting from GUARDIN knockdown (Supplementary Fig. 6b). These results indicate that GUARDIN plays an important part in both HR and NHEJ. In support, GUARDIN knockdown markedly enhanced doxorubicin-induced apoptosis in HCT116 cells, but had only moderate effects on responses to other stimuli (Fig. 7a,b).

We further examined the role of TRF2 and BRCA1 in GUARDIN-mediated protection of DNA integrity. Neither overexpression of TRF2, anti-miR-23a nor BRCA1 alone significantly affected the inhibition of DDR activation caused by GUARDIN knockdown (Supplementary Fig. 6c). However, co-overexpression of TRF2 and BRCA1 abolished the reduction in DDR activation following GUARDIN depletion, which was recapitulated by the co-introduction of anti-miR-23a and BRCA1-expressing constructs (Supplementary Fig. 6c). Thus, both TRF2 and BRCA1 are necessary for GUARDIN-mediated maintenance of DNA integrity. Consistently, the combination of TRF2 overexpression or anti-miR-23a and BRCA1 overexpression was necessary to abolish the inhibition of apoptosis and colony formation caused by knockdown of GUARDIN (Fig. 7c,d and Supplementary Fig. 6d).

Discussion

The role of p53 in maintaining genomic integrity has largely been attributed to its 'gatekeeper' function, arresting cell cycle progres-

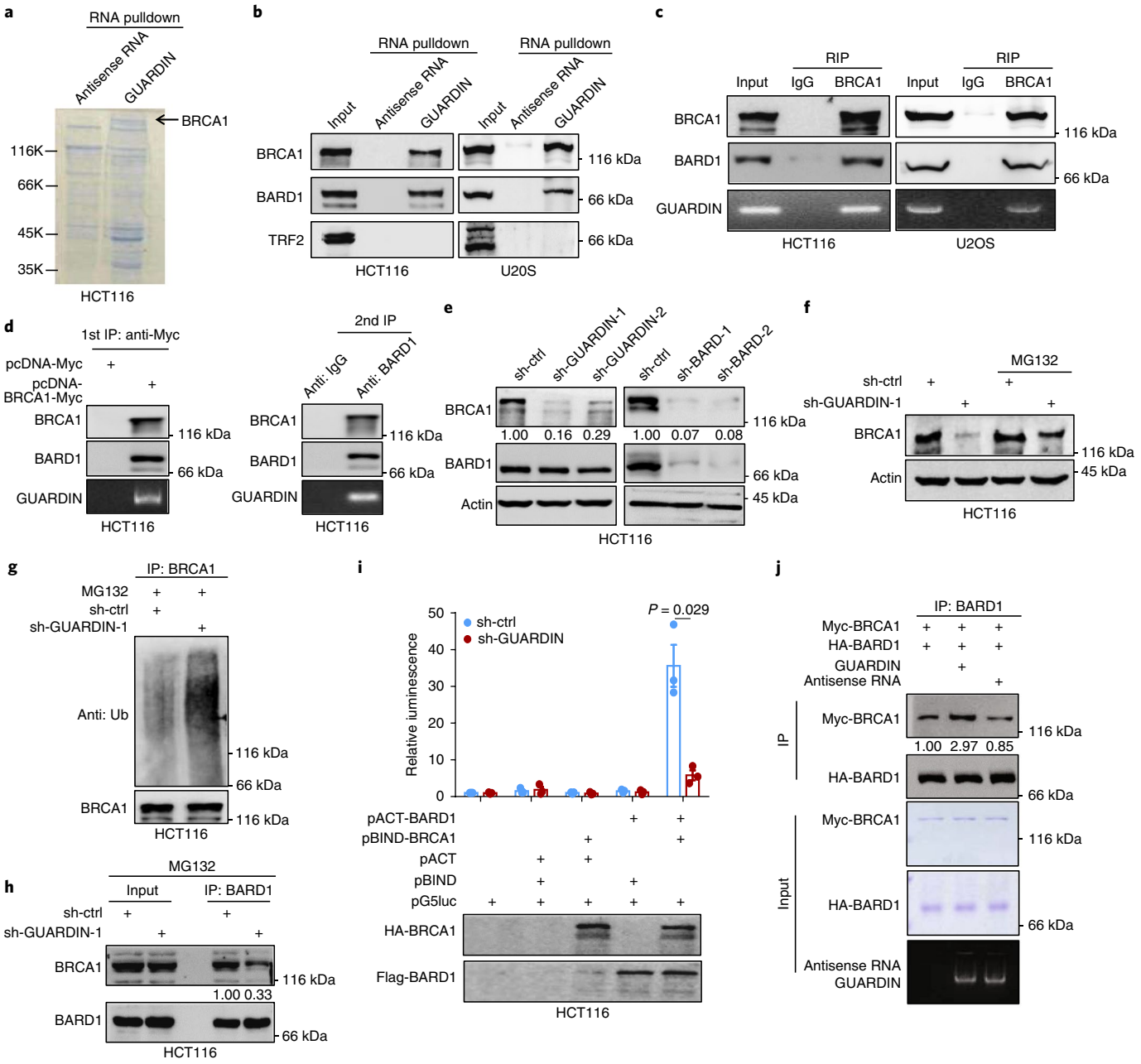

Fig. 5 | GUARDIN binds to and stabilizes BRCA1. a, A ~250 kDa protein band specifically pulled down by in vitro-transcribed biotin-labelled GUARDIN in total protein extracts of HCT116 cells was subsequently identified as BRCA1 using mass spectrometry. Data shown represent three independent experiments. **b**, BRCA1 and BARD1 were pulled down by biotin-labelled GUARDIN but not GUARDIN antisense RNA in whole-cell lysates of HCT116 and U2OS cells. Data shown represent three independent experiments. **c**, BARD1 and GUARDIN were co-precipitated with BRCA1 in whole-cell lysates of HCT116 and U2OS cells. Data shown represent three independent experiments. **d**, BRCA1, BARD1 and GUARDIN were co-precipitated with an anti-Myc antibody in whole-cell lysates of HCT116 cells transfected with Myc-tagged BRCA1 (left), and after elution with Myc peptide, all were further co-precipitated with an anti-BARD1 antibody in the resultant precipitates (right). Data shown represent three independent experiments. **e**, Silencing of GUARDIN, similar to silencing of BARD1, caused reduction in BRCA1 expression in HCT116 cells. Numbers represent the relative intensities of western blotting bands of BRCA1. Data shown represent three independent experiments. **f**, Downregulation of BRCA1 caused by silencing of GUARDIN was diminished by MG132 in HCT116 cells. Data shown represent three independent experiments. **g**, Silencing of GUARDIN resulted in increased polyubiquitination of BRCA1 in HCT116 cells. Data shown represent three independent experiments. Ub, ubiquitin. **h**, Silencing of GUARDIN caused reduction in the association between BRCA1 and BARD1 as shown in co-immunoprecipitation assays. Numbers represent the relative intensities of western blotting bands of BARD1. Data shown represent three independent experiments. **i**, Silencing GUARDIN caused reduction in the association between BRCA1 and BARD1 as shown in mammalian two-hybrid assays. Data are shown as mean ± s.e.m.; $n = 3$ independent experiments, two-tailed Student's t-test. HA, haemagglutinin. **j**, GUARDIN promoted the binding between recombinant BRCA1 and BARD1 in vitro. Numbers represent the relative intensities of western blotting bands of Myc-tagged BRCA1. Data shown represent three independent experiments. Statistics source data for **i** are provided in Supplementary Table 7. Uncropped images of blots for **b**–**j** are shown in Supplementary Fig. 7.

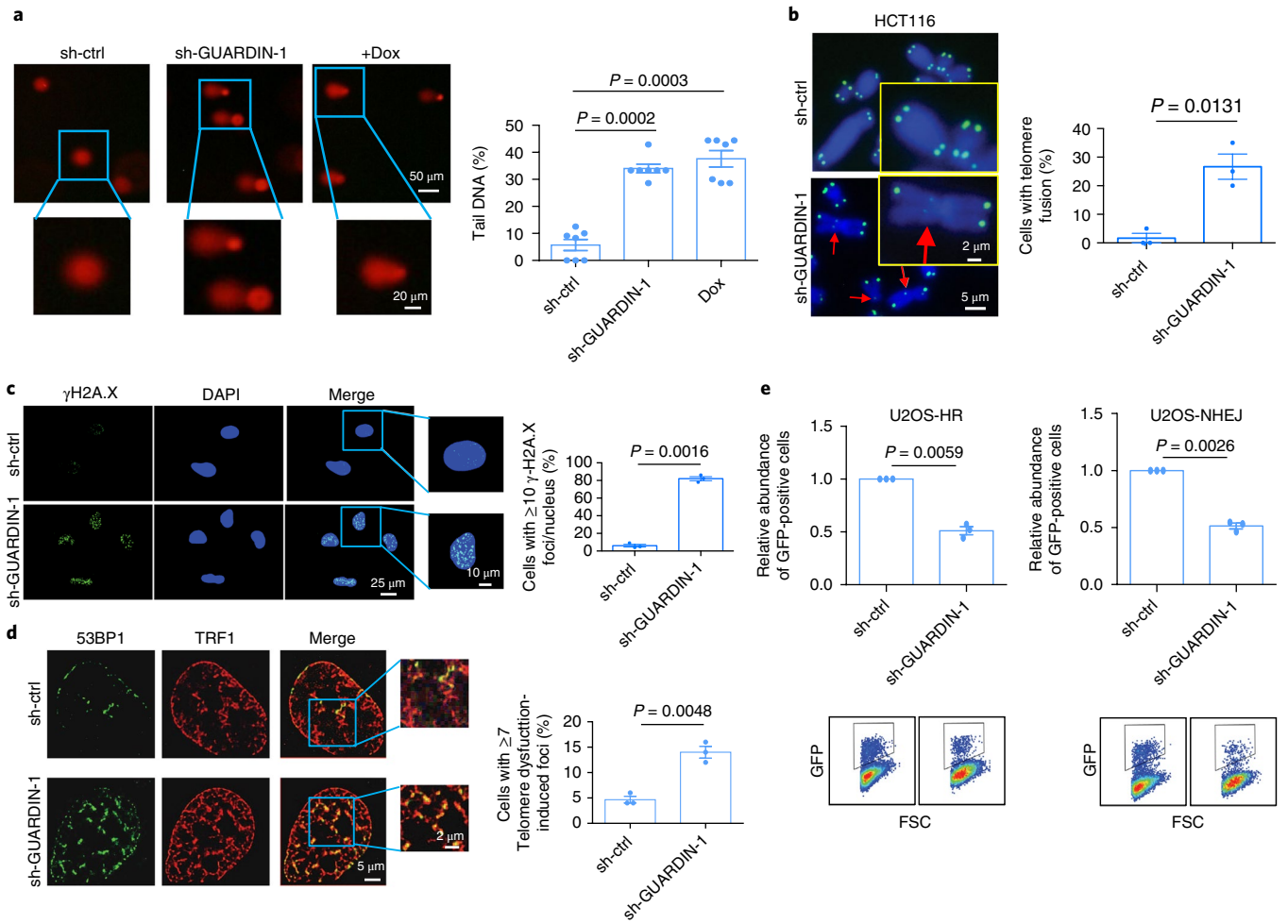

Fig. 6 | GUARDIN protects genomic integrity through TRF2 and BRCA1. a, Silencing of GUARDIN, similar to treatment with doxorubicin (Dox), caused DNA damage as shown by the appearance of comet tails in HCT116 cells. Data are shown as mean ± s.e.m.; $n = 7$ independent experiments, two-tailed Student's *t*-test. **b**, Silencing of GUARDIN caused telomere fusion in HCT116 cells. Red arrows denote fused telomeres revealed by FISH. Data are shown as mean ± s.e.m.; $n = 3$ independent experiments, two-tailed Student's *t*-test. **c**, Silencing of GUARDIN triggered the formation of γH2A.X foci (green) in HCT116 cells. Data are shown as mean ± s.e.m.; $n = 3$ independent experiments, two-tailed Student's *t*-test. **d**, Silencing of GUARDIN triggered the accumulation of 53BP1 (green) that is co-localized with TRF1 (red). Data are shown as mean ± s.e.m.; $n = 3$ independent experiments, two-tailed Student's *t*-test. **e**, Silencing of GUARDIN for 24 h caused reduction in the activation of the HR and NHEJ DNA repair pathways. FSC, forward scatter. Data are shown as mean ± s.e.m.; $n = 3$ independent experiments, two-tailed Student's *t*-test. Statistics source data for **a**–**e** are provided in Supplementary Table 7.

sion and allowing sufficient time to repair DNA damage or, upon irreversible DNA damage, to eliminate cells through apoptosis[33,34]. In this study, we identified the lncRNA GUARDIN as a p53-inducible effector that is critical for guarding the de novo structure of DNA. Although several p53-responsive lncRNAs that participate in the DDR are now documented[17], GUARDIN is distinguished by its pleotropic role both in DNA repair and in preventing telomere ends from being recognized as double-strand DNA breaks (Supplementary Fig. 6e). Thus, apart from facilitating DNA repair and eradicating severely damaged cells upon genotoxic insults, p53 has an active role in genome protection. Noticeably, although GUARDIN expression was primarily regulated by wild-type p53, it was detectable in *TP53*-null cells and in tumours with mutations in *TP53*, albeit at low levels (Fig. 2a–d and Supplementary Fig. 1a). Given that p53 inactivation through mutation or deletion occurs in >50% of human cancers[42], this proposes that unidentified mechanisms may be involved in the regulation of GUARDIN, and conceivably, GUARDIN may function independently of p53, as described recently for p21 (refs [1,43]). Moreover, the location of *GUARDIN* at the *FRA1A* fragile site suggests that it is susceptible to repression by genomic instability and therefore may act a tumour suppressor similar to co-located genes, such as miR-34a[44,45].

Silencing of GUARDIN triggered apoptosis and senescence commonly associated with DDR activation, typical manifestations of p53 responses to severe DNA damage[46]. However, inhibition of p53 did not have a similar effect on cell survival, even though it reduced the expression of GUARDIN. p53 is known to activate a broad transcriptional programme that results in the activation of genes necessary for DNA repair as well those required for the induction of apoptosis and senescence[47]. Thus, although GUARDIN inhibition removes an important pro-survival mechanism of the p53 pathway, it leaves anti-survival signalling intact. By contrast, p53 inhibition concurrently removes anti-survival signalling[48]. Thus, the functional hierarchy between p53 and GUARDIN involves p53 controlling the function of GUARDIN through regulating its expression, whereas GUARDIN in turn protects cells from the cytotoxic effect of p53.

We identified TRF2 as the effector through which GUARDIN functions as a safeguard to prevent the activation of the DDR at telomere ends. As a member of the shelterin complex, TRF2 along

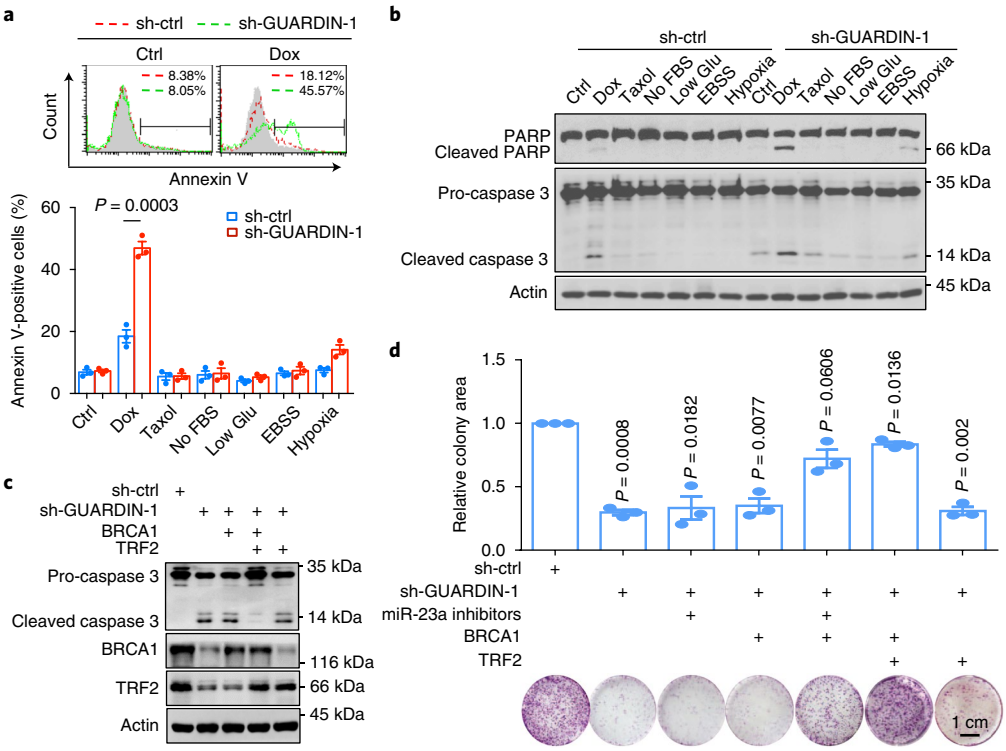

Fig. 7 | GUARDIN protects cells from apoptosis induced by genotoxic insults through TRF2 and BRCA1. a, Silencing of GUARDIN enhanced apoptosis induced by treatment with doxorubicin, but had only moderate effects on apoptosis induced by taxol, serum starvation (no FBS), glucose deprivation (low Glu), amino acid starvation (EBSS) and hypoxia. Data are shown as mean ± s.e.m.; $n = 3$ independent experiments, two-tailed Student's *t*-test. **b**, Silencing of GUARDIN enhanced the activation of caspase 3 and cleavage of poly(ADP-ribose) polymerase (PARP) caused by treatment with doxorubicin, but not by taxol, serum starvation, glucose deprivation, amino acid starvation and hypoxia. Data shown represent three independent experiments. **c**, Co-overexpression of TRF2 and BRCA1, but not overexpression TRF1 or BRCA1 alone, diminished the activation of caspase 3 caused by silencing of GUARDIN in HCT116 cells. Data shown represent three independent experiments. **d**, Silencing of GUARDIN inhibited the clonogenic potential of HCT116 cells, which was reversed by co-overexpression of TRF2 and BRCA1 or the co-introduction of anti-miR-23a and BRCA1-expressing constructs. Data are shown as mean ± s.e.m.; $n = 3$ independent experiments, two-tailed Student's *t*-test. Statistics source data for **a** and **d** are provided in Supplementary Table 7. Uncropped images of blots for **b** and **c** are shown in Supplementary Fig. 7.

with TRF1 are directly responsible for double-stranded DNA binding[11]. TRF2 inhibition uncaps telomeres that in turn activates the DDR, leading to the accumulation of telomere dysfunction-induced foci[49]. Indeed, GUARDIN knockdown recapitulated the formation of telomere dysfunction-induced foci associated with the downregulation of TRF2 (ref. [49]). This seemed to be due to relief of miR-23a sequestration by GUARDIN, allowing *TRF2* mRNA to be targeted[35]. Thus, GUARDIN, similar to other lncRNAs, functions as an intrinsic molecular sponge for miRNAs[33], promoting TRF2 expression epigenetically through competing for binding with miR-23a. Intriguingly, the number of molecules of GUARDIN detected in cells was ~2–4-fold fewer than miR-23a in individual cells (~70–150 GUARDIN versus ~180–400 miR-23a molecules), implying insufficient stoichiometric amounts of GUARDIN to sponge miR-23a. Nevertheless, the predicted multivalence of GUARDIN towards miR-23a indicates that GUARDIN can plausibly sponge and repress multiple miR-23a molecules.

The effector through which GUARDIN promoted the repair of damaged DNA seemed to be BRCA1, which has an important role in repairing double-strand DNA breaks[50,51]. Although BRCA1 is regulated by multiple genetic and epigenetic mechanisms[52,53], heterodimerization with BARD1 is known to be essential for BRCA1 stabilization[38,39]. Our results now demonstrate that GUARDIN is critically required for the association between BRCA1 and BARD1 as shown by: (1), GUARDIN, BRCA1 and BARD1 formed a ternary structure; (2), silencing of GUARDIN diminished the association between BRCA1 and BARD1 and inhibited BRCA1 expression; and (3) GUARDIN binds to BRCA1 and BARD1 with distinct structural regions. Thus, GUARDIN acts as an RNA scaffold to facilitate the association between BRCA1 and BARD1. Interestingly, a previous quantitative proteomic study in U2OS cells showed that, although BRCA1 was present with ~40,000 molecules per cell, BARD1 was expressed at a lower abundance of <500 molecules[54]. It is conceivable that the stoichiometric amounts of GUARDIN (~70–150 molecules per cell) are adequate for scaffolding of the BRCA1–BARD1 complex.

Consistent with sustained DNA damage in living cells, both HR and NHEJ DNA repair pathways were found to be constitutively activated. This was closely associated with the expression of GUARDIN, as silencing of GUARDIN attenuated the activation of HR and NHEJ. However, these findings are intriguing given that the reduction in TRF2 expression caused by GUARDIN silencing would conceivably cause increased activation of HR and NHEJ pathways as reported[7]. Nevertheless, the decrease in BRCA1 expression simultaneously resulting from GUARDIN inhibition would attenuate the activation of HR and NHEJ[55]. Although BRCA1 is primarily involved in HR in most studies[56–58], its role in NHEJ has also been reported[59,60]. Regardless, our results clearly demonstrate that GUARDIN deficiency causes damage to DNA through reduced TRF2 expression and by compromising DNA repair mediated by BRCA1. Thus, both TRF2 and BRCA1 are necessary for the maintenance of DNA integrity mediated by GUARDIN and cooperatively function to regulate cell survival and proliferation (Supplementary Fig. 6e).

A practical implication of this study is the potential application in cancer. Silencing of GUARDIN not only induced apoptosis but also rendered cancer cells more sensitive to genotoxic drugs. Of particular interest, molecularly targeted drugs that interfere with DNA repair mechanisms are emerging as a class of cancer therapeutics[61]. As a precedent, the poly(ADP-ribose) polymerase inhibitors are effective in the treatment of subsets of cancers that harbour mutant BRCA1 (refs [62,63]). Identification of small molecules that block the interaction of GUARDIN with miR-23a and BRCA1 will be of great interest towards applications in the treatment of cancer.

Methods

Methods, including statements of data availability and any associated accession codes and references, are available at https://doi.org/10.1038/s41556-018-0066-7.

Received: 9 February 2017; Accepted: 15 February 2018;
Published online: 28 March 2018

References

1. Hoeijmakers, J. H. J. DNA damage, aging, and cancer. *N. Engl. J. Med.* **361**, 1475–1485 (2009).
2. Hoeijmakers, J. H. J. The key role of DNA damage on cancer, aging and longevity. *Environ. Mol. Mutagen.* **53**, S13 (2012).
3. Braig, M. & Schmitt, C. A. Oncogene-induced senescence: putting the brakes on tumor development. *Cancer Res.* **66**, 2881–2884 (2006).
4. Best, B. P. Nuclear DNA damage as a direct cause of aging. *Rejuvenation Res.* **12**, 199–208 (2009).
5. Lahtz, C. & Pfeifer, G. P. Epigenetic changes of DNA repair genes in cancer. *J. Mol. Cell Biol.* **3**, 51–58 (2011).
6. Xin, H. W., Liu, D. & Zhou, S. Y. The telosome/shelterin complex and its functions. *Genome Biol.* **9,** 232 (2008).
7. Palm, W. & de Lange, T. How shelterin protects mammalian telomeres. *Annu. Rev. Genet.* **42,** 301–334 (2008).
8. Liu, D., O'Connor, M. S., Qin, J. & Songyang, Z. Telosome, a mammalian telomere-associated complex formed by multiple telomeric proteins. *J. Biol. Chem.* **279**, 51338–51342 (2004).
9. Fumagalli, M. et al. Telomeric DNA damage is irreparable and causes persistent DNA-damage-response activation. *Nat. Cell Biol.* **14**, 355–365 (2012).
10. van Tuyn, J. & Adams, P. D. Signalling the end of the line. *Nat. Cell Biol.* **14**, 339–341 (2012).
11. Martinez, P. & Blasco, M. A. Role of shelterin in cancer and aging. *Aging Cell* **9**, 653–666 (2010).
12. Majidinia, M. & Yousefi, B. DNA damage response regulation by microRNAs as a therapeutic target in cancer. *DNA Repair* **47**, 1–11 (2016).
13. Idogawa, M. et al. Identification and analysis of large intergenic non-coding RNAs regulated by p53 family members through a genome-wide analysis of p53-binding sites. *Hum. Mol. Genet.* **23**, 2847–2857 (2014).
14. Huarte, M. et al. A large intergenic noncoding RNA Induced by p53 mediates global gene repression in the p53 response. *Cell* **142**, 409–419 (2010).
15. Schmitt, A. M. et al. An inducible long noncoding RNA amplifies DNA damage signaling. *Nat. Genet.* **48**, 1370–1376 (2016).
16. Di Micco, R. et al. Oncogene-induced senescence is a DNA damage response triggered by DNA hyper-replication. *Nature* **444**, 638–642 (2006).
17. Léveillé, N. et al. Genome-wide profiling of p53-regulated enhancer RNAs uncovers a subset of enhancers controlled by a lncRNA. *Nat. Commun.* **27**, 6520 (2015).
18. Wang, W., Cheng, B., Miao, L., Mei, Y. & Wu, M. Mutant p53-R273H gains new function in sustained activation of EGFR signaling via suppressing miR-27a expression. *Cell Death Dis.* **4**, e574 (2013).
19. Tsang, W. P., Ho, F. Y., Fung, K. P., Kong, S. K. & Kwok, T. T. p53-R175H mutant gains new function in regulation of doxorubicin-induced apoptosis. *Int. J. Cancer* **114**, 331–336 (2005).
20. Liu, D. P., Song, H. & Xu, Y. A common gain of function of p53 cancer mutants in inducing genetic instability. *Oncogene* **29**, 949–956 (2010).
21. Jiang, P. et al. p53 regulates biosynthesis through direct inactivation of glucose-6-phosphate dehydrogenase. *Nat. Cell Biol.* **13**, 310–316 (2011).
22. Georgakilas, A. G. et al. Are common fragile sites merely structural domains or highly organized "functional" units susceptible to oncogenic stress? *Cell. Mol. Life Sci.* **71**, 4519–4544 (2014).
23. Henrich, K. O., Schwab, M. & Westermann, F. 1p36 tumor suppression—a matter of dosage? *Cancer Res.* **72**, 6079–6088 (2012).
24. Hunten, S. et al. p53-regulated networks of protein, mRNA, miRNA, and lncRNA expression revealed by integrated pulsed stable isotope labeling with amino acids in cell culture (pSILAC) and next generation sequencing (NGS) analyses. *Mol. Cell. Proteom.* **14**, 2609–2629 (2015).
25. Ashouri, A. et al. Pan-cancer transcriptomic analysis associates long non-coding RNAs with key mutational driver events. *Nat. Commun.* **7**, 13197 (2016).
26. Sarkar, S. et al. Different combinations of genetic/epigenetic alterations inactivate the p53 and pRb pathways in invasive human bladder cancers. *Cancer Res.* **60**, 3862–3871 (2000).
27. Vikhanskaya, F., Lee, M. K., Mazzoletti, M., Broggini, M. & Sabapathy, K. Cancer-derived p53 mutants suppress p53-target gene expression—potential mechanism for gain of function of mutant p53. *Nucleic Acids Res.* **35**, 2093–2104 (2007).
28. Li, Q. et al. C23 promotes tumorigenesis via suppressing p53 activity. *Oncotarget.* **7**, 58274–58285 (2016).
29. Debacq-Chainiaux, F., Erusalimsky, J. D., Campisi, J. & Toussaint, O. Protocols to detect senescence-associated β-galactosidase (SA-β-gal) activity, a biomarker of senescent cells in culture and in vivo. *Nat. Protoc.* **4**, 1798–1806 (2009).
30. Dimri, G. P. et al. A biomarker that identifies senescent human-cells in culture and in aging skin in vivo. *Proc. Natl Acad. Sci. USA* **92**, 9363–9367 (1995).
31. Sharma, V. et al. A BRCA1-interacting lncRNA regulates homologous recombination. *EMBO Rep.* **16**, 1520–1534 (2015).
32. Kartha, R. V & Subramanian, S. Competing endogenous RNAs (ceRNAs): new entrants to the intricacies of gene regulation. *Front. Genet.* **5,** 8 (2014).
33. Tay, Y., Rinn, J. & Pandolfi, P. P. The multilayered complexity of ceRNA crosstalk and competition. *Nature* **505**, 344–352 (2014).
34. Dodd, D. W., Gagnon, K. T. & Corey, D. R. Digital quantitation of potential therapeutic target RNAs. *Nucleic Acid. Ther.* **23**, 188–194 (2013).
35. Luo, Z. H. et al. mir-23a induces telomere dysfunction and cellular senescence by inhibiting TRF2 expression. *Aging Cell* **14**, 391–399 (2015).
36. Choi, K. H., Farrell, A. S., Lakamp, A. S. & Ouellette, M. M. Characterization of the DNA binding specificity of shelterin complexes. *Nucleic Acids Res.* **39**, 9206–9223 (2011).
37. Yan, Y., Liang, Z., Du, Q., Yang, M. & Geller, D. A. MicroRNA-23a downregulates the expression of interferon regulatory factor-1 in hepatocellular carcinoma cells. *Oncol. Rep.* **36**, 633–640 (2016).
38. Baer, R. & Ludwig, T. The BRCA1/BARD1 heterodimer, a tumor suppressor complex with ubiquitin E3 ligase activity. *Curr. Opin. Genet. Dev.* **12**, 86–91 (2002).
39. Hashizume, R. et al. The RING heterodimer BRCA1–BARD1 is a ubiquitin ligase inactivated by a breast cancer-derived mutation. *J. Biol. Chem.* **276**, 14537–14540 (2001).
40. Brzovic, P. S., Rajagopal, P., Hoyt, D. W., King, M. C. & Klevit, R. E. Structure of a BRCA1–BARD1 heterodimeric RING–RING complex. *Nat. Struct. Biol.* **8**, 833–837 (2001).
41. Shrivastav, M., De Haro, L. P. & Nickoloff, J. A. Regulation of DNA double-strand break repair pathway choice. *Cell Res.* **18**, 134–147 (2008).
42. Vogelstein, B., Lane, D. & Levine, A. J. Surfing the p53 network. *Nature* **408**, 307–310 (2000).
43. Galanos, P. et al. Chronic p53-independent p21 expression causes genomic instability by deregulating replication licensing. *Nat. Cell Biol.* **18**, 777–789 (2016).
44. Yin, D. et al. miR-34a functions as a tumor suppressor modulating EGFR in glioblastoma multiforme. *Oncogene* **32**, 1155–1163 (2013).
45. Okada, N. et al. A positive feedback between p53 and miR-34 miRNAs mediates tumor suppression. *Genes Dev.* **28**, 438–450 (2014).
46. Wynford-Thomas, D. p53: guardian of cellular senescence. *J. Pathol.* **180**, 118–121 (1996).
47. Stiewe, T. The p53 family in differentiation and tumorigenesis. *Nat. Rev. Cancer* **7,** 165–168 (2007).
48. Karlseder, J., Broccoli, D., Dai, Y. M., Hardy, S. & de Lange, T. p53- and ATM-dependent apoptosis induced by telomeres lacking TRF2. *Science* **283,** 1321–1325 (1999).
49. Takai, H., Smogorzewska, A. & de Lange, T. DNA damage foci at dysfunctional telomeres. *Curr. Biol.* **13,** 1549–1556 (2003).
50. Wang, Y. et al. BASC, a super complex of BRCA1-associated proteins involved in the recognition and repair of aberrant DNA structures. *Genes Dev.* **14**, 927–939 (2000).
51. Friedenson, B. The BRCA1/2 pathway prevents hematologic cancers in addition to breast and ovarian cancers. *BMC Cancer* **7,** 152 (2007).
52. Tapia, T. et al. Promoter hypermethylation of BRCA1 correlates with absence of expression in hereditary breast cancer tumors. *Epigenetics* **3**, 157–163 (2008).
53. Shen, J., Ambrosone, C. B. & Zhao, H. Novel genetic variants in microRNA genes and familial breast cancer. *Int. J. Cancer* **124**, 1178–1182 (2009).

54. Beck, M. et al. The quantitative proteome of a human cell line. *Mol. Syst. Biol.* **7**, 549 (2011).
55. Badie, S. et al. BRCA1 and CtIP promote alternative non-homologous end-joining at uncapped telomeres. *EMBO J.* **34**, 410–424 (2015).
56. Isono, M. et al. BRCA1 directs the repair pathway to homologous recombination by promoting 53BP1 dephosphorylation. *Cell Rep.* **18**, 520–532 (2017).
57. Powell, S. N. & Kachnic, L. A. Roles of BRCA1 and BRCA2 in homologous recombination, DNA replication fidelity and the cellular response to ionizing radiation. *Oncogene* **22**, 5784–5791 (2003).
58. Feng, Z. & Zhang, J. A dual role of BRCA1 in two distinct homologous recombination mediated repair in response to replication arrest. *Nucleic Acids Res.* **40**, 726–738 (2012).
59. Bau, D. T., Mau, Y. C. & Shen, C. Y. The role of BRCA1 in non-homologous end-joining. *Cancer Lett.* **240**, 1–8 (2006).
60. Jiang, G. et al. BRCA1–Ku80 protein interaction enhances end-joining fidelity of chromosomal double-strand breaks in the G1 phase of the cell cycle. *J. Biol. Chem.* **288**, 8966–8976 (2013).
61. Brown, J. S., O'Carrigan, B., Jackson, S. P. & Yap, T. A. Targeting DNA repair in cancer: beyond PARP inhibitors. *Cancer Discov.* **7**, 20–37 (2017).
62. Audeh, M. W. et al. Oral poly(ADP-ribose) polymerase inhibitor olaparib in patients with BRCA1 or BRCA2 mutations and recurrent ovarian cancer: a proof-of-concept trial. *Lancet* **376**, 245–251 (2010).
63. Tutt, A. et al. Oral poly(ADP-ribose) polymerase inhibitor olaparib in patients with BRCA1 or BRCA2 mutations and advanced breast cancer: a proof-of-concept trial. *Lancet* **376**, 235–244 (2010).

Acknowledgements

We thank X. Xu of Shenzhen University for providing U2OS-HR and U2OS-NHEJ cells and T. Ohta of St. Marianna University for providing the HA-BARD1 plasmid. We thank L. Kong and Q. Cheng of Henan Provincial People's Hospital for their assistance with preparation of tissue sections and immunohistochemistry experiments. This work was supported by grants from the National Key R&D Program of China (2016YFC1302302) and the National Natural Science Foundation of China (81430065, 31371388, 31601117 and 81471551).

Author contributions

W.L.H., L.J., A.X., X.D.Z. and M.W. designed the research. W.L.H., L.J. and A.X. performed most of the experiments and data analysis. Y.F.W. participated in the experiments and data analysis. R.F.T. participated in the data analysis and manuscript preparation. M.W., R.F.T. and X.D.Z. wrote the manuscript.

Competing interests

The authors declare no competing interests.

Additional information

Supplementary information is available for this paper at https://doi.org/10.1038/s41556-018-0066-7.

Reprints and permissions information is available at www.nature.com/reprints.

Correspondence and requests for materials should be addressed to X.D.Z. or M.W.

Publisher's note: Springer Nature remains neutral with regard to jurisdictional claims in published maps and institutional affiliations.

Methods

Cell culture and human tissues. HCT116, U2OS, A549, H1299, 293T and HAFF cells were maintained in DMEM (Invitrogen) supplemented with 10% FBS and 1% penicillin/streptomycin. Cells were cultured in a humidified incubator at 37 °C and 5% CO_2 and were tested using RT–PCR for mycoplasma contamination. Cell line authentication was performed using the AmpFISTR Identifiler PCR Amplification Kit from Applied Biosystems and GeneMarker V1.91 software (SoftGenetics LLC)[64]. Formalin-fixed paraffin-embedded (FFPE) colon cancer tissues were retrieved from the Department of Pathology at Henan Provincial People's Hospital (Zhengzhou, China). Freshly removed colon cancer and paired adjacent non-cancerous colon tissues were obtained from patients undergoing surgical resection at the Department of General Surgery at Henan Provincial People's Hospital. Studies using human tissues were approved by the Human Research Ethics Committees of the University of Science and Technology of China and Henan Provincial People's Hospital in agreement with the guidelines set forth by the Declaration of Helsinki. The study is compliant with all relevant ethical regulations for human research participants, and all participants provided written informed consent.

Antibodies and reagents. Information on antibodies used in this study is provided in Supplementary Table 6. The specificity of antibodies against p53, BRCA1, BARD1 and TRF2 was validated by short hairpin RNA (shRNA) knockdown experiments integrated in the study. MG132 was purchased from Calbiochem; doxorubicin, PFTα, z-VAD-fmk and doxycycline were obtained from Sigma-Aldrich; miR-23a mimics and inhibitors were purchased from GenePharma. Primers used are listed in Supplementary Tables 4,5.

***TP53* mutational status.** Analysis of *TP53* mutational status was carried out using a multiplex PCR kit for human *TP53* exons according to the manufacturer's instructions (Bio SB). This kit amplifies exons 2–4, exons 5–6, exons 7–9 and exons 10–11 of *TP53* from genomic DNA, comprising the complete coding region of *TP53*. The PCR primers have similar melting temperatures (Tm) and no obvious 3′-end overlap. The kit generates the 1,143-base pair (bp; exons 10–11), 777-bp (exons 7–9), 535-bp (exons 2–4) and 392-bp (exons 5–6) PCR products that were subjected to DNA sequencing.

In vitro transcription. The DNA template used for in vitro synthetization of biotinylated GUARDIN was generated by PCR amplification. The forward primer contained the T7 RNA polymerase promoter sequence to allow for subsequent in vitro transcription. PCR products were purified using the DNA Gel Extraction Kit (AxyPrep), and in vitro transcription was performed using the T7-Flash Biotin-RNA Transcription Kit (Epicentre) according to the manufacturer's instructions.

Biotin RNA pulldown assay. RNA pulldown assays were performed as previously described[49]. Briefly, cell lysates were prepared by ultrasonication in RIP buffer (150 mM KCl, 25 mM Tris (pH 7.4), 0.5 mM dithiothreitol, 0.5% NP-40, complete protease inhibitors cocktail and RNase inhibitors) and pre-cleared against streptavidin magnetic beads (Invitrogen). In vitro transcribed RNA adsorbed to streptavidin magnetic beads were then incubated with cell lysate at 4 °C for 4 h before washing five times in RIP buffer and elution in Laemmli sample buffer. Eluted proteins were separated by SDS–PAGE for mass spectrometry or western blotting.

Cytosolic/nuclear fractionation. Cells were incubated with hypotonic buffer (25 mM Tris–HCl (pH 7.4), 1 mM $MgCl_2$ and 5 mM KCl) on ice for 5 min. An equal volume of hypotonic buffer containing 1% NP-40 was then added, and the sample was left on ice for another 5 min. After centrifugation at 5,000*g* for 5 min, the supernatant was collected as the cytosolic fraction. The pellets were resuspended in nuclear resuspension buffer (20 mM HEPES (pH 7.9), 400 mM NaCl, 1 mM EDTA, 1 mM EGTA, 1 mM dithiothreitol and 1 mM phenylmethyl sulfonyl fluoride) and incubated at 4 °C for 30 min. The nuclear fraction was collected after removal of insoluble membrane debris by centrifugation at 12,000*g* for 10 min.

Biotin-miRNA pulldown assay. The miRNA pulldown assay was performed as previously described[50]. In brief, cells were transfected with biotin-miR-23a or biotin-scramble (GenePharma). After 24 h, cells were lysed in RIP buffer (150 mM KCl, 25 mM Tris (pH 7.4), 0.5 mM dithiothreitol, 0.5% NP-40, protease inhibitors cocktail and RNase inhibitors). Cell lysates were mixed with streptavidin magnetic beads in RIP buffer and incubated at 4 °C for 4 h. Beads were then washed five times with RIP buffer. RNA bound to the beads was isolated using TRIzol reagent (Invitrogen) and quantified by qRT–PCR.

Mammalian two-hybrid assays. Mammalian two-hybrid assays were performed using an assay kit according to the manufacturer's instructions (Promega E2440). Briefly, BRCA1 and BARD1 complementary DNA were cloned into the pBIND and pACT vectors to generate fusion proteins with the DNA-binding domain of GAL4 and the activation domain of VP16, respectively. The pBIND vector, which constitutively expressed the Renilla reniformis luciferase via the SV40 promoter, was used for normalization of transfection efficiency. The pG5luc vector contained five GAL4-binding sites upstream of the firefly luciferase gene, which was expressed when BRCA1-GAL4 bound to BRAD1-VP16. The pGAL4-BRCA1 and pVP16-BARD1 constructs were transfected along with the pG5luc vector into cells. Two days later, firefly and Renilla luciferase activity was measured by the Dual-Luciferase Reporter Assay System (Promega), and Renila activity was used to normalize firefly luciferase activity.

Electrophoretic mobility shift assay. Electrophoretic mobility shift assay was performed according to the manufacturer's protocol of the LightShift Chemiluminescent RNA EMSA Kit (Thermo Scientific). In brief, the biotin end-labelled GUARDIN RNA with BARD1 or BRCA1 proteins were incubated in the binding reaction system. Reactions were subjected to gel electrophoresis on a native polyacrylamide gel and transferred to nylon membranes. The biotin end-labelled RNA was detected using the streptavidin horseradish peroxidase conjugate and chemiluminescent substrate.

Chromatin immunoprecipitation assays. Chromatin immunoprecipitation assays were performed by using the Millipore ChIP kit (17-371RF) according to the manufacturer's instructions. Bound DNA fragments were subjected to real-time PCR using specific primers (Supplementary Table 4).

Luciferase reporter assays. Luciferase reporter assays were performed according to the manufacturer's instructions (Promega). Cells were transfected with the pGL3-based constructs containing the *GUARDIN* promoter together with Renilla luciferase plasmids. To evaluate the interaction between miR-23a and GUARDIN, cells were transfected with psiCHECK2-based constructs containing GUARDIN-WT or GUARDIN-MUT plus miR-23a mimics or inhibitors. Twenty-four hours later, firefly and Renilla luciferase activity was examined by the Dual-Luciferase Reporter Assay System, and Renilla activity was used to normalize firefly activity.

Absolute quantitation of GUARDIN and miR-23a. Absolute RNA quantitation was performed using a Bio-Rad QX100 Digital Droplet PCR system[65]. cDNA preparation was carried out using the TaqMan MicroRNA Reverse Transcription Kit for miR-23a and qScript cDNA SuperMix for GUARDIN with 5 µl of DNase-treated RNA (corresponding to RNA derived from 0.5 million cells) in a 20 µl reaction and subsequently diluted to 200 µl. Given the aforementioned dilutions, cDNA concentration was calculated to be at 2,500 cell equivalents of template per µl. The PCR solution was reconstituted to a final volume of 25 µl using 1–5 µl of template and Digital Droplet PCR Supermix (Bio-Rad). Droplet formation was carried out using a QX100 droplet generator, and the emulsion cycled to end point as per the manufacturer's protocol. Samples were then read using a Bio-Rad QX100 reader. Data from the droplet reader are given as copies per µl and were converted to copies per cell based on the known cell equivalents of input cDNA. Primers/probes for the detection of GUARDIN and miR-23a were designed and synthesized by Applied Biosystems.

Immunofluorescence staining. Cells grown on coverslips were fixed in 4% paraformaldehyde, permeabilized in 0.2% Triton X-100 and incubated overnight at 4 °C with the following primary antibodies: γH2A.X (Cell Signaling), 53BP1 (Novus) and TRF1 (Abcam). Secondary antibodies raised against rabbit were labelled with Alexa Fluor 488 or Alexa Fluor 568. Samples were observed under a fluorescence microscope (γH2A.X) (Zeiss) or a SR GSD 3D microscope (53BP1 and TRF1) (Leica). For quantitation of γH2A.X foci, cells with ≥10 γH2A.X foci were recorded as positive. The percentage of γH2A.X-positive cells were calculated from five random fields (×10 objective). For quantitation of telomere dysfunction-induced foci, cells with ≥7 53BP1 foci co-localized with TRF1 foci were considered positive. The percentage of telomere dysfunction-induced foci-positive cells were calculated from 50 random cells.

Comet assays. The comet assays were performed according to the manufacturer's instructions (Trevigen#4250-050-K). Briefly, 500 cells (1×10^5 cells per ml) were mixed with low-melting-point agarose on the comet slides at 37 °C. After solidifying for 10 min at 4 °C, the slides were immersed in the lysis solution for 2 h and then in freshly prepared akaline unwinding solution to permit DNA unfolding for 1 h at 4 °C. Slides were then subjected to electrophoresis (21 V for 30 min). The slides were washed with ddH_2O twice, immersed in 75% ethanol for 5 min, stained with propidium iodide and then observed under a fluorescence microscope. The percentage of tail DNA content of the comet was measured with Comet Assay IV software (Perceptive Instruments)[66].

Cell viability. The CellTiter-Glo Luminescent Cell Viability Assay Kit (Promega) was used according to the manufacturer's instructions. Briefly, cells were seeded at 5×10^3 per well in 96-well plates overnight before treatment as desired. CellTiter-Glo Reagent (100 ml) was added and incubated for 10 min before recording luminescence on a Synergy 2 multidetection microplate reader (BioTek)[67].

Apoptosis. Apoptotic cells were quantitated using the Annexin V Apoptosis Detection Kit (BD Biosciences). In brief, cells were washed twice with cold PBS and then resuspended in binding buffer at a concentration of 1×10^6 cells per ml.

100 µl of the solution (1×10^5 cells) were transferred to a 5-ml culture tube and 5 µl of annexin V was added. After incubation at room temperature for 15 min in the dark, an additional 400 µl of binding buffer was added to each tube, and cells were analysed using a flow cytometer within 1 h (FACSCanto, BD Biosciences).

Cell cycle analysis. Cells were fixed by 70% ethanol on ice for 1 h and spun down at 4,000 r.p.m. Cell pellets were resuspended in PBS containing 0.25% Triton X-100 and incubated on ice for 15 min. After discarding the supernatant, the cell pellet was resuspended in 0.5 ml PBS containing 10 µg per ml RNase A and 20 µg per ml propidium iodide stock solution and incubated at room temperature in the dark for 30 min. Cells were then subjected to analysis using a flow cytometer (FACSCanto).

Senescence. Senescence was detected by staining senescence-associated β -galactosidase using a Senescence Detection Kit according to the manufacturer's instructions (C0602, Beyotime). The percentages of senescence-associated β -galactosidase-positive cells were calculated from five random fields under a light microscope (×10 objective).

Telomere fluorescence in situ hybridization analysis. Telomere fluorescence in situ hybridization (FISH) analysis was performed using the Telomere PNA FISH Kit/FITC (Agilent). In brief, sample DNA was denatured at 80 °C for 5 min under a coverslip in the presence of the fluorescein-conjugated peptide nucleic acid (PNA) probe. Hybridization was performed in the dark at room temperature for 30 min thereafter followed by a brief rinse with Rinse Solution, and a post-hybridization wash with Wash Solution at 65 °C for 5 min. Coverslips were mounted with 2×10 µl antifade reagent containing 4,6-diamidino-2-phenylindole (DAPI) as counterstain. Images were digitally recorded using epifluorescence microscopy using a FITC filter set.

Immunohistochemistry. Immunostaining was carried out as previously described[68]. Serial FFPE tissue sections (5 µm thick) were de-waxed and rehydrated. Antigen retrieval was performed in a pressure cooker for 20 min in 10 mM Tris with 1 mM EDTA (pH 9). Endogenous peroxidase activity was inhibited with 1.5% H_2O_2 in methanol for 20 min followed by washing in PBS. Nonspecific binding was blocked using blocking buffer (PBS (pH 7.4), 3% serum, 1% BSA and 0.1% Tween) for 60 min at room temperature. Sections were then incubated with primary antibodies (p53 and p21, Santa Cruz) that were diluted in blocking buffer overnight at 4 °C. After washing twice with 0.1% PBS–Tween, slides were incubated with a secondary antibody (Cell Signaling Technology). After washing, sections were incubated with with 3,3′-diaminobenzidine (DAB) (Sigma-Aldrich) followed by counterstaining with haematoxylin (Sigma-Aldrich). After dehydration, sections were mounted using Cytoseal 60 (Thermo Scientific). Slides were examined by two investigators. The percentage of positive cells was estimated from 0% to 100%. The intensity of staining (intensity score) was judged on an arbitrary scale of 0–4: no staining (0), weakly positive staining (1), moderately positive staining (2), strongly positive staining (3) and very strongly positive staining (4). An immunoreactive score was derived by multiplying the percentage of positive cells with staining intensity divided by 10.

In situ hybridization. FFPE tissue sections (5 µm thick) were deparaffinized followed by treatment with 10% hydrogen peroxide and pepsin (2 ug per ml, EXIQON) for 1 h at 37 °C. Sections were then incubated with hybridization solution with digoxigenin (DIG)-labelled probes at 42 °C for 24 h (10 ug per ml, synthesized by Shengong). After washing with 5× SSC (Gibco) for 10 min, 2× SSC for 10 min and 0.2× SSC at 55 °C for 10 min each wash, sections were incubated with blocking buffer (PBST with 10% normal goat serum and 5% BSA) at 37 °C for 1 h. This was followed by incubation with an anti-DIG antibody at 4 °C for 12 h. After washing, sections were incubated with horseradish peroxidase-coupled second antibody at room temperature for 1 h followed by incubation with DAB. Counterstaining was carried out using nuclear fast red solution before dehydration. The slides were examined by two investigators. The percentage of positive cells was estimated from 0% to 100%. The intensity of staining was judged on an arbitrary scale of 0–4, as previously mentioned (see 'Immunohistochemistry' section). A reactive score was derived by multiplying the percentage of positive cells with staining intensity divided by 10. HCT116 cells with or without GUARDIN knocked down by shRNA grown on coverslips were included as positive or negative biological control.

Laser capture microdissection. Freshly removed colon cancer tissues and paired adjacent non-cancerous colon tissues were mounted in Tissue-Tek OCT compound (Sakura Finechemicals) and frozen. Each sample was then cut into 10–20 serial sections with a thickness of 10 µm. Sections were mounted on uncoated glass slides. After cancer cells were identified using haematoxylin–eosin staining, they were microdissected according to the standard laser capture procedure using a PixCell II LCM system (Arcturus Engineering/Olympus). Total RNA was extracted from laser-captured cell nests by using the PicoPure RNA Isolation Kit according to the manufacturer's protocol, including on-column DNase treatment (Qiagen).

Two-step immunoprecipitation. All processes were performed under RNase-free conditions. Immunoprecipitation was carried out as described previously[51]. Briefly, HCT116 cells with or without Myc-tagged BRCA1 transfection were lysed in buffer containing 20 mM HEPES (pH 7.8), 400 mM KCl, 5% glycerol, 5 mM EDTA, 1% NP40, protease inhibitors cocktail and RNase inhibitor. Cell lysates were first immunoprecipitated with anti-Myc antibody. Ten per cent of the immunoprecipitates was analysed by western blotting and RT–PCR analysis. The remaining immunoprecipitates were then eluted with Myc peptides. The eluent was further incubated with control IgG or anti-BARD1 antibody for a second immunoprecipitation assay, followed by western blot and RT–PCR analysis.

Colony formation assay. HCT116 cells transduced with the control of GUARDIN shRNA were transfected with either miR-23a inhibitors, TRF2 or BRCA1 as indicated. Twenty-four hours later, 1×10^3 cells were cultured in a 6-well plate. Two weeks later, cells were fixed, stained with crystal violet and photographed. The percentage and intensity of the area covered by crystal violet-stained cell colonies were quantified using the ImageJ-plugin 'ColonyArea'[69].

Protein purification. Haemagglutinin-tagged BARD1 or Myc-tagged BRCA1 was expressed in 293T cells. Proteins were purified using A/G-Sepharose bead-bound antibodies against haemagglutinin and Myc. The immunoprecipitates were then eluted with haemagglutinin and Myc peptides.

Xenograft mouse model. HCT116 cells expressing the control or GUARDIN shRNA were subcutaneously injected into the dorsal flanks of 4-week-old male BALB/c nu/nu mice (6 mice per group, Shanghai SLAC Laboratory Animal Co. Ltd.). Four weeks later, mice were killed, and tumours were excised and measured. Studies on animals were approved by the Animal Research Ethics Committee of the University of Science and Technology of China and were conducted in accordance with relevant guidelines and regulations.

RNA interference. Gene knockdown with shRNA was performed as previously described[52]. Briefly, HEK293T cells were transfected with shRNAs (cloned in PLKO.1), gag/pol, rev and VSVG plasmids with the ratio of 2/2/2/1. Twenty-four hours after transfection, cells were cultured in fresh medium for an additional 24 h. The culture medium containing lentiviral particles was centrifuged at 1,000*g* for 5 min and the supernatant was used for infection. shRNA sequences are shown in Supplementary Table 5.

lncRNA microarray. The expression of lncRNAs was determined using Arraystar Human LncRNA Microarray v3.0 (KangChen Bio-tech). The sample preparation and microarray hybridization were performed based on the manufacturer's standard protocols with minor modifications. Briefly, mRNA was purified from total RNA after the removal of rRNA (mRNA-ONLY Eukaryotic mRNA Isolation Kit, Epicentre). Each sample was amplified and transcribed into fluorescent cRNA along the entire length of the transcripts without 3′ bias utilizing a random priming method. The labelled cRNAs were hybridized onto the Human LncRNA Array v3.0 (8×60 K). After washing the slides, arrays were scanned using an Agilent G2505C Scanner.

Statistics and reproducibility. Each experiment was repeated independently with similar results at least three times, except for the experiments shown in Figs. 2b–e and 3d,e and Supplementary Fig. 2b,c,h, which were repeated twice. Statistical analysis was carried out using Microsoft Excel software and GraphPad Prism to assess the differences between experimental groups. Statistical significance was analysed by two-tailed Student's *t*-test and expressed as a *P* value. $P<0.05$ were considered to be statistical significance.

Life Sciences Reporting Summary. Further information on experimental design is available in the Life Sciences Reporting Summary.

Data availability. lncRNA microarray data that support the findings of this study have been deposited in the Gene Expression Omnibus (GEO) under accession code GSE95186. Source data for Figs. 1a–g,i,j, 2b–e,h, 3a–c,e–g, 4a–h, 5i, 6a–e and 7a,d and Supplementary Figs. 1a,c–f, 2b–e,h, 3a,c and 6a–d have been provided as Supplementary Table 7. All other data supporting the findings of this study are available from the corresponding author on reasonable request.

References

64. Dong, L. et al. Ets-1 mediates upregulation of Mcl-1 downstream of XBP-1 in human melanoma cells upon ER stress. *Oncogene* **30**, 3716–3726 (2011).
65. Dodd, D. W., Gagnon, K. T. & Corey, D. R. Digital quantitation of potential therapeutic target RNAs. *Nucleic Acid. Ther.* **23**, 188–194 (2013).
66. Karbaschi, M. & Cooke, M. S. Novel method for the high-throughput processing of slides for the comet assay. *Sci. Rep.* **4,** 7200 (2014).
67. Liu, X. Y. et al. RIP1 kinase is an oncogenic driver in melanoma. *Cancer Res.* **75**, 1736–1748 (2015).
68. Jin, L. et al. MicroRNA-149*, a p53-responsive microRNA, functions as an oncogenic regulator in human melanoma. *Proc. Natl Acad. Sci. USA* **108**, 15840–15845 (2011).
69. Guzman, C., Bagga, M., Kaur, A., Westermarck, J. & Abankwa, D. ColonyArea: an ImageJ plugin to automatically quantify colony formation in clonogenic assays. *PLoS ONE* **9**, e92444 (2014).

nature research

Corresponding author(s): Mian Wu

☐ Initial submission ☐ Revised version ☒ Final submission

Life Sciences Reporting Summary

Nature Research wishes to improve the reproducibility of the work that we publish. This form is intended for publication with all accepted life science papers and provides structure for consistency and transparency in reporting. Every life science submission will use this form; some list items might not apply to an individual manuscript, but all fields must be completed for clarity.

For further information on the points included in this form, see Reporting Life Sciences Research. For further information on Nature Research policies, including our data availability policy, see Authors & Referees and the Editorial Policy Checklist.

Experimental design

1. Sample size

   Describe how sample size was determined.

   For human samples, no statistical method was used to predetermine sample size due to the availability. For animal study, fig. 3d and 3e related experiment has n=6 independent mice per group.
   Unless explicitly stated, 3 independent experiments were performed to achieve Student's t-test analysis.

2. Data exclusions

   Describe any data exclusions.

   No data were excluded for this study.

3. Replication

   Describe whether the experimental findings were reliably reproduced.

   The shown experiments could successfully and reliably be replicated and reproduced.

4. Randomization

   Describe how samples/organisms/participants were allocated into experimental groups.

   Human samples were not randomized. For animal study, all the animals were randomly grouped for experiments.

5. Blinding

   Describe whether the investigators were blinded to group allocation during data collection and/or analysis.

   For experiments using cell lines the investigators were not blinded during data acquisition and analysis. The application of treatments and processing procedures negated the possibility of blinding but there was no human bias given all data was collected independently using instrumentation. Similarly, in the animal experiments the investigators were not blinded to the group allocation. Two observers measured volumes/weights to alleviate human bias in these data. For experiments involving human tissues, sample IDs were coded and the investigator was not aware of the group allocation during data acquisition. Group allocations were decoded afterwards for the purpose of data analysis.

Note: all studies involving animals and/or human research participants must disclose whether blinding and randomization were used.

6. Statistical parameters

For all figures and tables that use statistical methods, confirm that the following items are present in relevant figure legends (or in the Methods section if additional space is needed).

n/a	Confirmed
☐	☒ The exact sample size (*n*) for each experimental group/condition, given as a discrete number and unit of measurement (animals, litters, cultures, etc.)
☐	☒ A description of how samples were collected, noting whether measurements were taken from distinct samples or whether the same sample was measured repeatedly
☐	☒ A statement indicating how many times each experiment was replicated
☐	☒ The statistical test(s) used and whether they are one- or two-sided (note: only common tests should be described solely by name; more complex techniques should be described in the Methods section)
☒	☐ A description of any assumptions or corrections, such as an adjustment for multiple comparisons
☐	☒ The test results (e.g. *P* values) given as exact values whenever possible and with confidence intervals noted
☐	☒ A clear description of statistics including central tendency (e.g. median, mean) and variation (e.g. standard deviation, interquartile range)
☐	☒ Clearly defined error bars

See the web collection on statistics for biologists for further resources and guidance.

Software

Policy information about availability of computer code

7. Software

Describe the software used to analyze the data in this study.	Microsoft Excel 2010; GraphPad Prism V6; BD CellQuest™ Pro Software; Image J; LAS-4000 Image Reader software; SDS V2.4; AxioVision Microscopy Software; Comet Assay IV software

For manuscripts utilizing custom algorithms or software that are central to the paper but not yet described in the published literature, software must be made available to editors and reviewers upon request. We strongly encourage code deposition in a community repository (e.g. GitHub). *Nature Methods* guidance for providing algorithms and software for publication provides further information on this topic.

Materials and reagents

Policy information about availability of materials

8. Materials availability

Indicate whether there are restrictions on availability of unique materials or if these materials are only available for distribution by a for-profit company.	Plasmids used in this study are available for reasonable request. All other materials used are commercially available.

9. Antibodies

Describe the antibodies used and how they were validated for use in the system under study (i.e. assay and species).	All antibodies are listed in Supplementary Table 6 with species, company/catalog#, clone and dilution used per application. β-actin (YT0099) and BARD1 (YT0452) were purchased from Immunoway. PARP-1 (SC-8007), p53 (SC-126), GAPDH (sc-32233) and BARD1 (SC-74559; 2 µg/mg lysate for Immunoprecipitation) were purchased from Santa Cruz Biotechnology. IRF1 (11335-1-AP; 1:500 dilution) and TRF2 (22020-1-AP; 1:500 dilution) were from Proteintech. GAPDH (AT0002) was from CMCTAG. 53BP1 (NB100-304; 1:500 dilution) was from Novusbio. p21 (P1484; 1:2000 dilution), Flag (F-3165; 1:2000 dilution), HA (H-9658; 1:2000 dilution) were from Sigma. TRF1 (ab10579; 1:500 dilution), Digoxigenin (ab420), BRCA1 (ab16780; 2 µg/mg lysate for Immunoprecipitation) were from Abcam. Ub (#3936), Phospho-Histone H2A.X (Ser139) (#9718; 1:200 dilution for Immunofluorescence), Caspase-3 (#9665; 1:500 dilution) and BRCA1 (#9010; 1:500 dilution) were from Cell Signaling Technology. p53 (21891-1-AP, 1:500 for Immunohistochemistry) and p21 (10355-1-AP, 1:500 for Immunohistochemistry) were from Proteintech. Unless indicated, all the antibodies were used in 1:1000 dilution. The commercial antibodies were validated based on the information on the manufacturers' instructions. Additional validation was done by the use of siRNA- treated samples as negative control.

10. Eukaryotic cell lines

a. State the source of each eukaryotic cell line used.

HCT116, U2OS, A549, H1299, and 293T cell lines were purchased from ATCC. HAFF (human adult foreskin fibroblast) cells were isolated in the lab.

b. Describe the method of cell line authentication used.

Individual cell line authentication was confirmed using the AmpFISTR Identifiler PCR Amplification Kit from Applied Biosystems and GeneMarker V1.91 software (SoftGenetics LLC).

c. Report whether the cell lines were tested for mycoplasma contamination.

All of the cells used were regularly tested for mycoplasma contamination

d. If any of the cell lines used are listed in the database of commonly misidentified cell lines maintained by ICLAC, provide a scientific rationale for their use.

No commonly misidentified cell lines were used.

Animals and human research participants

Policy information about studies involving animals; when reporting animal research, follow the ARRIVE guidelines

11. Description of research animals

Provide details on animals and/or animal-derived materials used in the study.

All animal studies were conducted in accordance with relevant guidelines and regulations and were approved by the Animal Research Ethics Committee of the University of Science and Technology of China. BALB/c nude mice, male, 4-week old were purchased from Shanghai SLAC Laboratory Animal Co. Ltd.

Policy information about studies involving human research participants

12. Description of human research participants

Describe the covariate-relevant population characteristics of the human research participants.

A cohort of 100 colon cancer patients with stages I to IV colon cancer were collected at the Henan Provincial People's Hospital. This cohort were composed of 56 males and 44 females from 35 to 75 years old (median: 58 years old).
A cohort of 40 colon cancer patients with stages I and II colon cancer were collected at the Henan Provincial People's Hospital. This cohort were composed of 24 males and 16 females from 36 to 72 years old (median: 58 years old).

nature research

Corresponding author(s): Mian Wu

☐ Initial submission ☒ Revised version ☐ Final submission

Flow Cytometry Reporting Summary

Form fields will expand as needed. Please do not leave fields blank.

Data presentation

For all flow cytometry data, confirm that:

☒ 1. The axis labels state the marker and fluorochrome used (e.g. CD4-FITC).

☒ 2. The axis scales are clearly visible. Include numbers along axes only for bottom left plot of group (a 'group' is an analysis of identical markers).

☒ 3. All plots are contour plots with outliers or pseudocolor plots.

☒ 4. A numerical value for number of cells or percentage (with statistics) is provided.

Methodological details

5. Describe the sample preparation.	Apoptosis analysis: Apoptotic cells were quantitated using Annexin V staining according to the manufacturer's protocol of Annexin V Apoptosis Detection Kit (BD Biosciences). In brief, cells were washed twice with cold PBS and then re-suspended in binding buffer at a concentration of 1 × 106 cells/ml. One hundred µl of the resulting solution (1 × 105 cells) were transferred to a 5-ml culture tube, and 5 µl of annexin V was added. After incubation at room temperature for 15 min in the dark, an additional 400µl of binding buffer were added to each tube, and cells were analysed using a flow cytometer within 1 h (FACSCanto, BD Biosciences). Cell cycle analysis: Cells were fixed by 70% Ethanol on ice for 1 hour and spun down at 4000 rpm. Cell pellets were re-suspended in PBS containing 0.25% Triton X-100 and incubate on ice for 15 min. Discard supernatant and re-suspend cell pellet in 0.5 ml PBS containing 10 µg/ml RNase A and 20 µg/ml PI stock solution and incubate at room temperature (RT) in the dark for 30 min. Cells were then subjected to analysis using a flow cytometer (FACSCanto, BD Biosciences).
6. Identify the instrument used for data collection.	BD FACSCanto flow cytometer.
7. Describe the software used to collect and analyze the flow cytometry data.	BD CellQuest™ Pro Software.
8. Describe the abundance of the relevant cell populations within post-sort fractions.	No sorting was employed.
9. Describe the gating strategy used.	Cells were gated based on forward and side scatter plots, only avoiding debris and aggregates and no extensive gating strategy was used.

Tick this box to confirm that a figure exemplifying the gating strategy is provided in the Supplementary Information. ☒